The Astrophysical Journal, 621:673–694, 2005 March 10

THE EPOCHS OF EARLY-TYPE GALAXY FORMATION AS A FUNCTION OF ENVIRONMENT

Daniel Thomas, Claudia Maraston, and Ralf Bender
Max-Planck-Institut für extraterrestrische Physik, Giessenbachstraße, D-85748 Garching, Germany;
and Universitäts-Sternwarte München, Scheinerstraße 1, D-81679 München, Germany

and

Claudia Mendes de Oliveira
Instituto Astronômico e Geofísico, Universidade de São Paulo, Rua do Matão 1226–Cidade Universitária, 05508-900 São Paulo SP, Brazil
Received 2004 June 30; accepted 2004 October 5

ABSTRACT

The aim of this paper is to set constraints on the epochs of early-type galaxy formation through the "archaeology" of the stellar populations in local galaxies. Using our models of absorption-line indices that account for variable abundance ratios, we derive ages, total metallicities, and element ratios of 124 early-type galaxies in high- and low-density environments. The data are analyzed by comparison with mock galaxy samples created through Monte Carlo simulations taking the typical average observational errors into account, in order to eliminate artifacts caused by correlated errors. We find that all three parameters, age, metallicity, and α/Fe ratio, are correlated with velocity dispersion. We show that these results are robust against recent revisions of the local abundance pattern at high metallicities. To recover the observed scatter we need to assume an intrinsic scatter of about 20% in age, 0.08 dex in [Z/H], and 0.05 dex in [α/Fe]. All low-mass objects with $M_* \lesssim 10^{10}\ M_\odot$ ($\sigma \lesssim 130$ km s^{-1}) show evidence for the presence of intermediate-age stellar populations with low α/Fe ratios. About 20% of the intermediate-mass objects with $10^{10} \lesssim M_*/M_\odot \lesssim 10^{11}$ [$110 \lesssim \sigma/(\mathrm{km\ s^{-1}}) \lesssim 230$; both elliptical and lenticular galaxies] must have either a young subpopulation or a blue horizontal branch. On the basis of the above relationships, valid for the bulk of the sample, we show that the Mg-σ relation is mainly driven by metallicity, with similar contributions from the α/Fe ratio (23%) and age (17%). We further find evidence for an influence of the environment on the stellar population properties. Massive early-type galaxies in low-density environments seem on average $\sim$2 Gyr younger and slightly ($\sim$0.05–0.1 dex) more metal-rich than their counterparts in high-density environments. No offsets in the α/Fe ratios are instead detected. With the aid of a simple chemical evolution model, we translate the derived ages and α/Fe ratios into star formation histories. We show that most star formation activity in early-type galaxies is expected to have happened between redshifts $\sim$3 and 5 in high-density environments and between redshifts 1 and 2 in low-density environments. We conclude that at least 50% of the total stellar mass density must have already formed at $z \sim 1$, in good agreement with observational estimates of the total stellar mass density as a function of redshift. Our results suggest that significant mass growth in the early-type galaxy population below $z \sim 1$ must be restricted to less massive objects, and a significant increase of the stellar mass density between redshifts 1 and 2 should be present, caused mainly by the field galaxy population. The results of this paper further imply the presence of vigorous star formation episodes in massive objects at $z \sim 2$–5 and evolved elliptical galaxies around $z \sim 1$, both observationally identified as SCUBA galaxies and extremely red objects, respectively.

Subject headings: galaxies: abundances — galaxies: elliptical and lenticular, cD — galaxies: evolution — galaxies: formation — galaxies: stellar content

Online material: machine-readable tables

1. INTRODUCTION

The most direct way to constrain the formation and evolution of galaxies certainly is to trace back their evolution with redshift (e.g., Aragón-Salamanca et al. 1993; Bender et al. 1996; Ziegler & Bender 1997; Stanford et al. 1998; Kodama et al. 1999; Poggianti et al. 1999; Ziegler et al. 1999; Kelson et al. 2000; van Dokkum et al. 2000; Saglia et al. 2000). The price to be paid, however, is that high-redshift data naturally have lower quality and are therefore more difficult to interpret. A clear complication is the so-called progenitor bias, which implies that galaxies observed at low and high redshift are not necessarily drawn from the same sample (van Dokkum et al. 2000). The alternative approach is the detailed investigation of the stellar populations in local galaxies, which has been pioneered by the analysis of slopes and scatter of color-magnitude and scaling relations of early-type galaxies (e.g., Dressler et al. 1987; Djorgovski & Davis 1987; Bower et al. 1992; Bender et al. 1992, 1993; Renzini & Ciotti 1993), followed by a number of detailed studies of absorption-line indices (e.g., Peletier 1989; Gorgas et al. 1990; Worthey et al. 1992; Davies et al. 1993, 2001; Carollo & Danziger 1994; Rose et al. 1994; Bender & Paquet 1995; Fisher et al. 1995; Jørgensen et al. 1995; Greggio 1997; Vazdekis et al. 1997; Tantalo et al. 1998; Kuntschner & Davies 1998; Mehlert et al. 1998, 2003; Worthey 1998; Kobayashi & Arimoto 1999; Vazdekis & Arimoto 1999; Jørgensen 1999; Terlevich et al. 1999; Kuntschner 2000; Kuntschner et al. 2001; Longhetti et al. 2000; Trager et al. 2000b; Poggianti et al. 2001a, 2001b; Carter et al. 2002; Proctor & Sansom 2002; Terlevich & Forbes 2002; Saglia et al. 2002; Cenarro et al. 2003; Caldwell et al. 2003; Thomas et al. 2003b; and others). We call this the "archaeology approach." The confrontation with predictions from models of galaxy formation is certainly most meaningful when the two approaches, the mining of the high-redshift universe and the archaeology of local

galaxies, set consistent constraints. In this paper we follow the latter approach.

The main challenge in the archaeology of stellar populations is the disentanglement of age and metallicity effects. The use of absorption-line indices is a powerful tool to lift this degeneracy (Faber et al. 1985; González 1993; Worthey 1994) but until now has been hampered by the fact that different metallic line indices yield different metallicities and therefore different ages (see references above). We have solved this problem by developing stellar population models that include element abundance ratio effects and now allow for an unambiguous derivation of age, total metallicity, and element ratios from (Lick) absorption-line indices (Thomas et al. 2003a, hereafter TMB). A complication that remains, however, is the degeneracy between age and horizontal branch morphology, which stems from the fact that the presence of warm horizontal branch stars (which cannot be excluded) strengthens the Balmer absorption and can mimic a younger stellar population age (de Freitas Pacheco & Barbuy 1995; Maraston & Thomas 2000; Lee et al. 2000). We discuss this problem at greater length in the present paper.

The principal aim of this study is to constrain the formation epochs of the stellar populations in early-type galaxies as a function of their type (elliptical and lenticular), mass, and environmental density. For this purpose we analyze a homogeneous, high-quality data sample of 124 early-type galaxies in various environmental densities. With our new stellar population models (TMB) we determine ages, total metallicities, and α/Fe ratios from the absorption-line indices Hβ, Mg b, and $\langle$Fe$\rangle$ and seek possible correlations of these parameters with velocity dispersion. First tentative results have already been discussed in Thomas et al. (2002). Here we present the final and more comprehensive analysis. In particular, we compare the observed data set with mock samples produced through Monte Carlo simulations taking the typical average observational errors into account, in order to eliminate the confusion caused by correlated errors (Trager et al. 2000b; Kuntschner et al. 2001; Terlevich & Forbes 2002).

The α/Fe element ratio plays a key role in the accomplishment of our main goal, namely, the derivation of formation epochs. While the so-called α-elements O, Ne, Mg, Si, S, Ar, Ca, and Ti (particles that are built up with α-particle nuclei) plus the elements N and Na are delivered mainly by Type II supernova explosions of massive progenitor stars, a substantial fraction of the Fe peak elements Fe and Cr comes from the delayed exploding Type Ia supernovae (e.g., Nomoto et al. 1984; Woosley & Weaver 1995; Thielemann et al. 1996). Hence, the α/Fe ratio quantifies the relative importance of Type II and Type Ia supernovae (Greggio & Renzini 1983; Matteucci & Greggio 1986; Pagel & Tautvaisiene 1995; Thomas et al. 1998) and therefore carries information about the timescale over which star formation occurs. Thus, the α/Fe ratio can be considered to be an additional measure of late star formation, and we use it both to constrain formation timescales and to lift the degeneracy between age and horizontal branch morphology.

The paper is organized as follows. In §§ 2 and 3 we present the methodology of the paper; i.e., we introduce the data sample, briefly summarize the stellar population model of TMB, and explain the construction of the mock galaxy sample through Monte Carlo simulations. The results of this analysis are presented in § 4. We use these results to explore the origin of the Mg-σ relation (§ 5) and derive star formation histories (§ 6) with the aim of constraining the epoch of early-type galaxy formation. The main results of the paper are discussed and summarized in §§ 7 and 8.

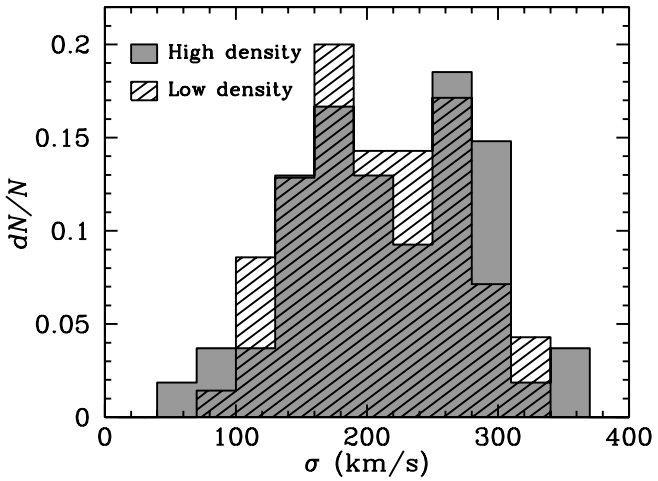

FIG. 1.—Distribution of central velocity dispersion in high-density (*gray histogram*) and low-density (*hatched histogram*) environments.

2. THE DATA SAMPLE

2.1. *Sample Selection*

We analyze a sample of 124 early-type galaxies, 70 of which reside in low-density and 54 in high-density environments, containing roughly equal fractions of elliptical and lenticular (S0) galaxies. To maintain statistical significance, in the following we make the rough bimodal distinction between low- and high-density environments. It should be emphasized that the classification "low density" comprises galaxies in environments with low density, not necessarily isolated objects. The sample is constructed from the following sources: 41 galaxies in high-density (Virgo Cluster) and low-density environments (González 1993), 32 Coma Cluster galaxies (Mehlert et al. 2000, 2003), and 51 galaxies (mostly low-density environment) from Beuing et al. (2002) selected from the ESO-LV catalog (Lauberts & Valentijn 1989; highest quality objects). In this latter sample, objects with a local galaxy surface density $NG_T > 9$ are assigned to the high-density environment. NG_T is given in Lauberts & Valentijn (1989) and is the number of galaxies per square degree inside a radius of 1° around the considered galaxy (see Beuing et al. 2002). The sample spans a large range in central velocity dispersion $60 \lesssim \sigma_0/(\mathrm{km\ s^{-1}}) \lesssim 340$, with similar distributions in both environments (Fig. 1).

In the data samples quoted above, absorption-line strengths are measured as functions of galaxy radius. We adopt the central indices determined within 1/10 of the effective radius, so that the analysis presented here does not suffer from aperture effects. We use the Lick indices Hβ, Mg b, and $\langle$Fe$\rangle$ = 0.5(Fe5270+ Fe5335) to derive the stellar population parameters age t, total metallicity [Z/H], and the element abundance ratio [α/Fe]. The medians of the 1 σ errors in Hβ, Mg b, Fe5270, and Fe5335 are 0.06, 0.06, 0.07, and 0.08 Å, respectively.

We have reobserved 19 objects of the Beuing et al. (2002) sample with the same telescope (the 1.5 m telescope on La Silla) with the principal aim of extending the wavelength range to the blue (C. Mendes de Oliveira et al. 2005, in preparation). We find a good agreement for the optical absorption-line indices Hβ, Mg b, and $\langle$Fe$\rangle$ between the two samples, with a small systematic offset in Mg b of 0.2 Å. Since the latter observations have

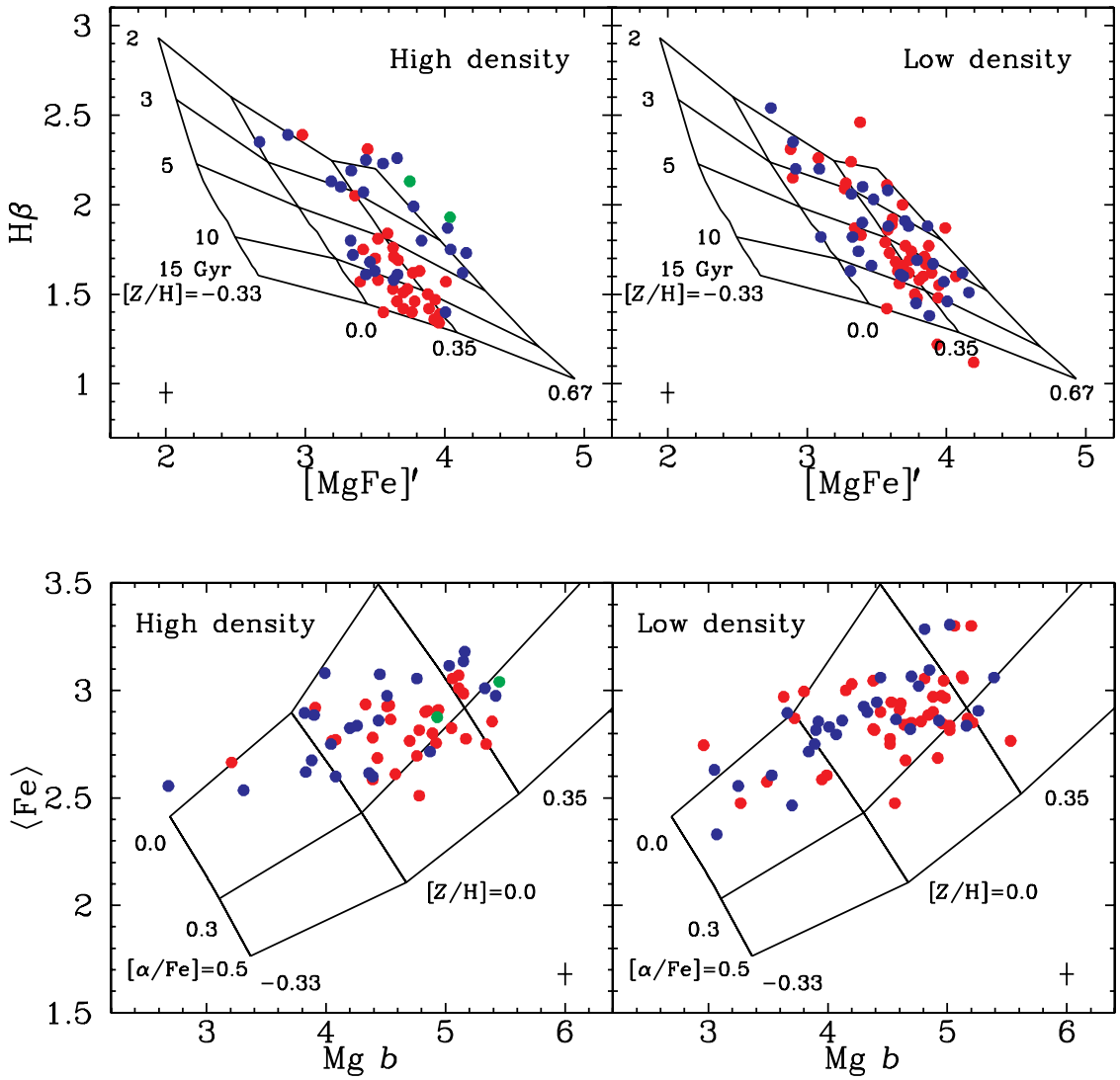

FIG. 2.—Lick indices $[\mathrm{MgFe}]'$ vs. Hβ (*top*) and Mg b vs. $\langle \mathrm{Fe} \rangle$ (*bottom*). Symbols represent the early-type galaxies analyzed in this paper, taken from González (1993), Beuing et al. (2002), and Mehlert et al. (2003). Index values are measured within $\sim 1/10 r_e$. Left and right panels show objects in high-and low-density environments, respectively. Red symbols represent elliptical, blue symbols lenticular, and green symbols cD galaxies. Median 1 σ error bars are shown. SSP models (TMB) with the metallicities $[Z/\mathrm{H}] = 0.0$, 0.35, and 0.67 are plotted for different ages $t = 2$, 3, 5, 10, and 15 Gyr at fixed α/Fe ratio ($[\alpha/\mathrm{Fe}] = 0$; *top*) and different α/Fe ratios $[\alpha/\mathrm{Fe}] = 0.0,\ 0.3,\ 0.5$ at fixed age ($t = 12$ Gyr; *bottom*) as indicated by the labels.

higher quality because of the installation of a new CCD chip and holographic grating, we corrected for the offset in Mg b and replaced the values of Beuing et al. (2002) with the new measurements for the objects in common. We emphasize here, however, that the results of this paper are not affected by this procedure.

2.2. *Absorption-Line Indices*

In Figure 2 we present the absorption-line index measurements plotting $[\mathrm{MgFe}]'$ versus Hβ (*top panels*) and Mg b versus $\langle \mathrm{Fe} \rangle$ (*bottom panels*). The index

$$[\mathrm{MgFe}]' = \sqrt{(\mathrm{Mg}\ b)(0.72 \times \mathrm{Fe5270} + 0.28 \times \mathrm{Fe5335})},$$

a slight modification of [MgFe] defined by González (1993), is almost completely independent of α/Fe ratio variations (TMB). Left and right panels show data in high- and low-density environments, respectively. Red symbols are elliptical, blue symbols are lenticular, and green symbols are cD galaxies. Overplotted are our stellar population models (TMB) for various ages, metallicities, and α/Fe ratios as indicated by the labels in the diagrams.

2.2.1. *TMB Models*

The TMB models take the effects from element abundance ratio changes on all Lick indices into account and hence give Lick indices of simple stellar populations (SSPs) not only as functions of age and metallicity but also as a function of the α/Fe ratio. They are based on the evolutionary population synthesis code of Maraston (1998, 2004). In Thomas et al. (2003a), the impact from element ratio changes is computed with the help of the Tripicco & Bell (1995) response functions, using an extension of the method introduced by Trager et al. (2000a). The updated version used in this paper adopts the new metallicity-dependent response functions from Korn et al. (2004). As discussed there, the impact of metallicity on the response functions for the indices considered here is negligible (see also Thomas et al. 2004) and hence does not affect the results of this paper.

Particular care was taken to calibrate the SSP models with globular cluster data (Maraston et al. 2003), which—most

importantly—include objects with relatively high, namely, solar, metallicities (Puzia et al. 2002). We match very well their Hβ, Mg b, and $\langle$Fe$\rangle$ indices with models in which the α/Fe ratio is enhanced by a factor of 2 relative to the solar value, in agreement with results from high-resolution spectroscopy of individual stars (see TMB and Maraston et al. 2003 and references therein). Because of the inclusion of element ratio effects, the models allow for the clear distinction between total metallicity [Z/H] and the α to iron peak elements ratio [α/Fe].

We use these models to derive the three stellar population parameters age, metallicity, and α/Fe ratio from the three line indices Hβ, Mg b, and $\langle$Fe$\rangle$ in a twofold iterative procedure explained below. As mentioned in § 1, there is a degeneracy between age and horizontal branch morphology. A way to lift this degeneracy is the consideration of the α/Fe ratio. We expect young stellar populations generally to be characterized by lower α/Fe ratios owing to the late enrichment of Fe from Type Ia supernovae.

In this paper we present a detailed investigation of the data set based on Monte Carlo simulations as is discussed in the following sections. However, first tentative conclusions can already be drawn by the direct comparison between the observational data and SSP model grids, as discussed in the following.

2.2.2. *Ages and Metallicities*

The index [MgFe]$'$ is a good tracer of total metallicity (still degenerate with age, of course), since it is almost completely independent of α/Fe ratio variations (TMB). Because Hβ is also only very slightly sensitive to α/Fe (TMB), the top panels of Figure 2 are well suited to read off ages and total metallicities independent of abundance ratio effects.

The sample splits into two subclasses divided by the Balmer absorption index at H$\beta \approx 2$ Å. The main part of the data is centered around H$\beta = 1.6$ Å, while about one-quarter of the objects have relatively high Hβ absorption, implying the presence of either young stellar populations or blue horizontal branch morphologies (Maraston & Thomas 2000). This surprisingly well-defined separation is also discussed in Mehlert et al. (2003) for the Coma Cluster objects alone. Interestingly, the pattern is still present for the larger galaxy sample considered here, and in particular the fraction of high-Hβ objects seems to be independent of the environmental density (Fig. 2), but we do not find a significant difference with respect to the galaxy type. Figure 2 further hints toward a difference between objects as a function of environment within the old (low Hβ) class, in the sense that galaxies in low-density environments seem to have on average slightly younger ages and higher metallicities. This difference is more clearly visible in the direct comparison of the derived ages discussed below.

2.2.3. *Element Abundance Ratios*

Figure 2 (*bottom*) can be used to get rough estimates for the α/Fe ratios of the sample galaxies. It should be emphasized, however, that the Mg b–$\langle$Fe$\rangle$ plane is not completely degenerate in age, and the ages derived from the top panels have to be taken into account for the precise derivation of α/Fe ratios. Nevertheless, we can infer from Figure 2 (*bottom*) that the α/Fe ratios range roughly between solar and 2 times solar and that objects with strong Mg b indices, hence velocity dispersion because of the Mg-σ relation (e.g., Bender et al. 1993), tend to have higher α/Fe ratios. At least no obvious impact from environmental density on the α/Fe ratios is visible.

2.2.4. *Derivation of Stellar Parameters*

The stellar population parameters are derived in a twofold iterative procedure. First, we arbitrarily fix the α/Fe ratio and determine ages and metallicities for the index pairs (Hβ, Mg b) and (Hβ, $\langle$Fe$\rangle$) by starting with arbitrary age-metallicity pairs, which we modify iteratively until both index pairs are reproduced. The two metallicities obtained from Mg b and $\langle$Fe$\rangle$, respectively, are used to adjust the α/Fe ratio and to start a new iteration. These steps are repeated until the age-metallicity pairs derived from (Hβ, Mg b) and (Hβ, $\langle$Fe$\rangle$) at a given α/Fe ratio are consistent within 1% accuracy. For ages and metallicities between the grid points quoted above, we interpolate linearly. The resulting ages, metallicities, and α/Fe for the sample under investigation are listed in Table 3.

3. THE MONTE CARLO APPROACH

An uncomfortable effect of the degeneracy between age and metallicity is that the errors of these stellar population parameters are not independent. It is still a matter of debate, for instance, whether the age-metallicity anticorrelation found for early-type galaxies in a number of studies is an artifact caused by correlated errors (Jørgensen 1999; Trager et al. 2000b; Poggianti et al. 2001b; Kuntschner et al. 2001; Terlevich & Forbes 2002; Proctor & Sansom 2002). A possibility to get a handle on these effects is the performance of Monte Carlo simulations, taking into account the observational uncertainties of the line indices from which the stellar population parameters are derived. Kuntschner et al. (2001) follow this method in order to assess the relationship between the ages and metallicities of 72 early-type galaxies by comparison with a mock sample produced through Monte Carlo simulations.

In this paper we extend the approach of Kuntschner et al. (2001) to the full parameter space including α/Fe ratios in addition to age and total metallicity. We produce a sample of artificial galaxies with given ages, metallicities, and α/Fe ratios, from which we compute with the TMB SSP models the line indices Hβ, Mg b, and $\langle$Fe$\rangle$. By means of Monte Carlo simulations we perturb these "exact" values with the 1 σ errors quoted above, assuming a Gaussian error distribution. An illustrative example for the resulting correlations between the errors of the three population parameters is given in Figure 3 for an artificial object with H$\beta = 1.59$ Å, Mg $b = 4.73$ Å, and $\langle$Fe$\rangle = 2.84$ Å, corresponding to an age of 10.7 Gyr, a metallicity [Z/H] $= 0.26$, and [α/Fe] $= 0.25$ indicated by the dotted lines. The circles are 100 Monte Carlo realizations taking the 1 σ errors in the line indices (dH$\beta = 0.06$ Å, dMg $b = 0.06$ Å, dFe5270 $= 0.07$ Å, and dFe5335 $= 0.08$ Å) into account.

The distributions of the resulting stellar population parameters can be well described by Gaussians. The corresponding 1 σ errors are 1.48 Gyr in age, 0.04 dex in total metallicity, and 0.02 dex in α/Fe ratio. We confirm that errors produce a very tight linear anticorrelation between log age and metallicity (Fig. 3, *top left*) as already mentioned above. Interestingly, we find that the errors of age and α/Fe ratio are also anticorrelated (Fig. 3, *bottom left*). This relationship is the result of the slightly stronger age dependence of the Mg b index with respect to $\langle$Fe$\rangle$, caused by the larger contribution from turnoff stars to Mg b and Mg_2 (Maraston et al. 2003). An underestimation of the age leads to the prediction of lower Mg indices relative to iron, which results in the derivation of a larger α/Fe ratio, and vice versa.

In the following, Monte Carlo simulations are used to reproduce and analyze the distribution of the data in the diagrams shown in Figure 2. The simulations are carried out in two steps; low- and high-density environments are considered separately throughout the analysis.

1. First, we seek correlations between galaxy velocity dispersion and the stellar population properties age, metallicity, and

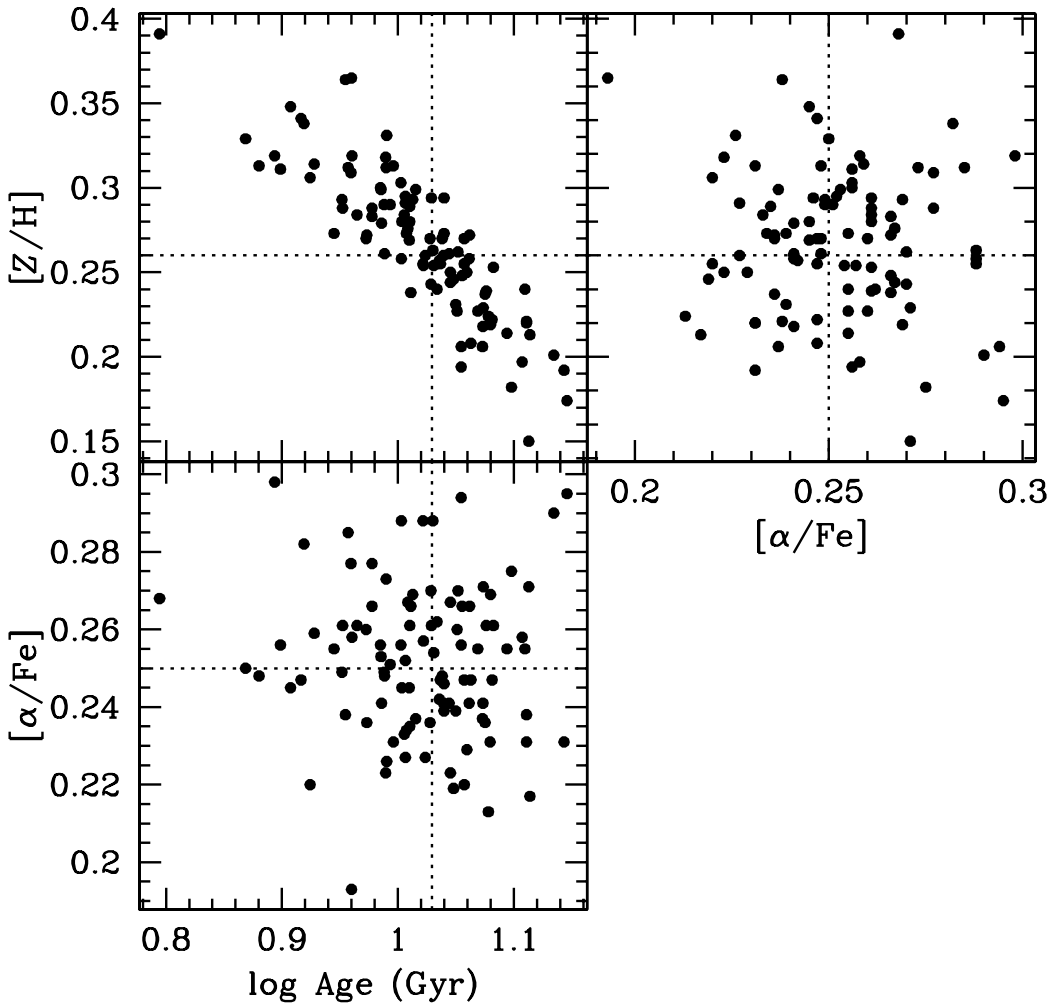

FIG. 3.—Stellar population parameters of an object with H$\beta = 1.59$ Å, Mg $b = 4.73$ Å, and $\langle$Fe$\rangle = 2.84$ Å, corresponding to an age of 10.7 Gyr, a metallicity $[Z/\mathrm{H}] = 0.26$, and $[\alpha/\mathrm{Fe}] = 0.25$ as indicated by the dotted lines. The circles represent Monte Carlo realizations perturbing the original index values with the 1 σ errors $d\mathrm{H}\beta = 0.06$ Å, dMg $b = 0.06$ Å, dFe5270 $= 0.07$ Å, and dFe5335 $= 0.08$ Å. The resulting 1 σ errors of the stellar population parameters are 1.48 Gyr in age, 0.04 dex in total metallicity, and 0.02 dex in α/Fe ratio.

α/Fe ratio that reproduce the majority of the data sample. Indeed, Trager et al. (2000b) have already shown that velocity dispersion is the only structural parameter that is found to modulate the stellar populations of galaxies. Because we aim at deriving average properties, simple stellar populations of single age and single chemical composition are used. We start with the velocity dispersion (σ) distribution of the data sample shown in Figure 1. On the basis of arbitrarily chosen relationships, we assign to every σ an age, metallicity, and α/Fe ratio, which we transform into Hβ, Mg b, and $\langle$Fe$\rangle$. These indices are then perturbed with the observational error (see above), adopting a Gaussian probability distribution. In this way we obtain a mock galaxy sample that is closest to the observational situation in terms of size, velocity dispersion distribution, and error perturbation. If necessary, we add an intrinsic scatter in the stellar population parameters age, metallicity, and α/Fe. This step is repeated until the majority of the observed data points in the index-index diagrams $[\mathrm{MgFe}]'$ versus Hβ and Mg b versus $\langle$Fe$\rangle$ are reproduced (comparison "by eye"). The quality of the fit is further checked with respect to the zero points, slopes, and scatter of the relationships between the stellar parameters (age, metallicity, and α/Fe ratio) and velocity dispersion. By means of the index-index diagrams we identify those objects that are not reproduced by the mock data sample based on the simple relationships introduced in this step.

2. In a second step, we therefore perturb the general simple scaling laws found in the first step in two-component models in order to match those remaining objects. As before, we adopt the exact σ-distribution of the outliers and assign age, metallicity, and α/Fe to every σ on the basis of the above final relationships to define the base population. Then we add a second component with arbitrary stellar population parameters and determine the index values of this composite population. These are then perturbed as in the first step and compared with the observational data. We note that the contribution in mass of the second component is treated as the fourth free parameter; hence, the solutions will not be unique, since we have only three observables as constraints (Hβ, Mg b, and $\langle$Fe$\rangle$). As discussed in detail below, we use plausibility arguments to try to maintain the astrophysical feasibility of the Monte Carlo realizations, in order to constrain the relative weights of the subcomponents.

4. RESULTS

In Figure 4 the comparison of our Monte Carlo realizations (*black symbols*) with the observational data (*colored symbols*) is shown in the index-index planes introduced with Figure 2. By

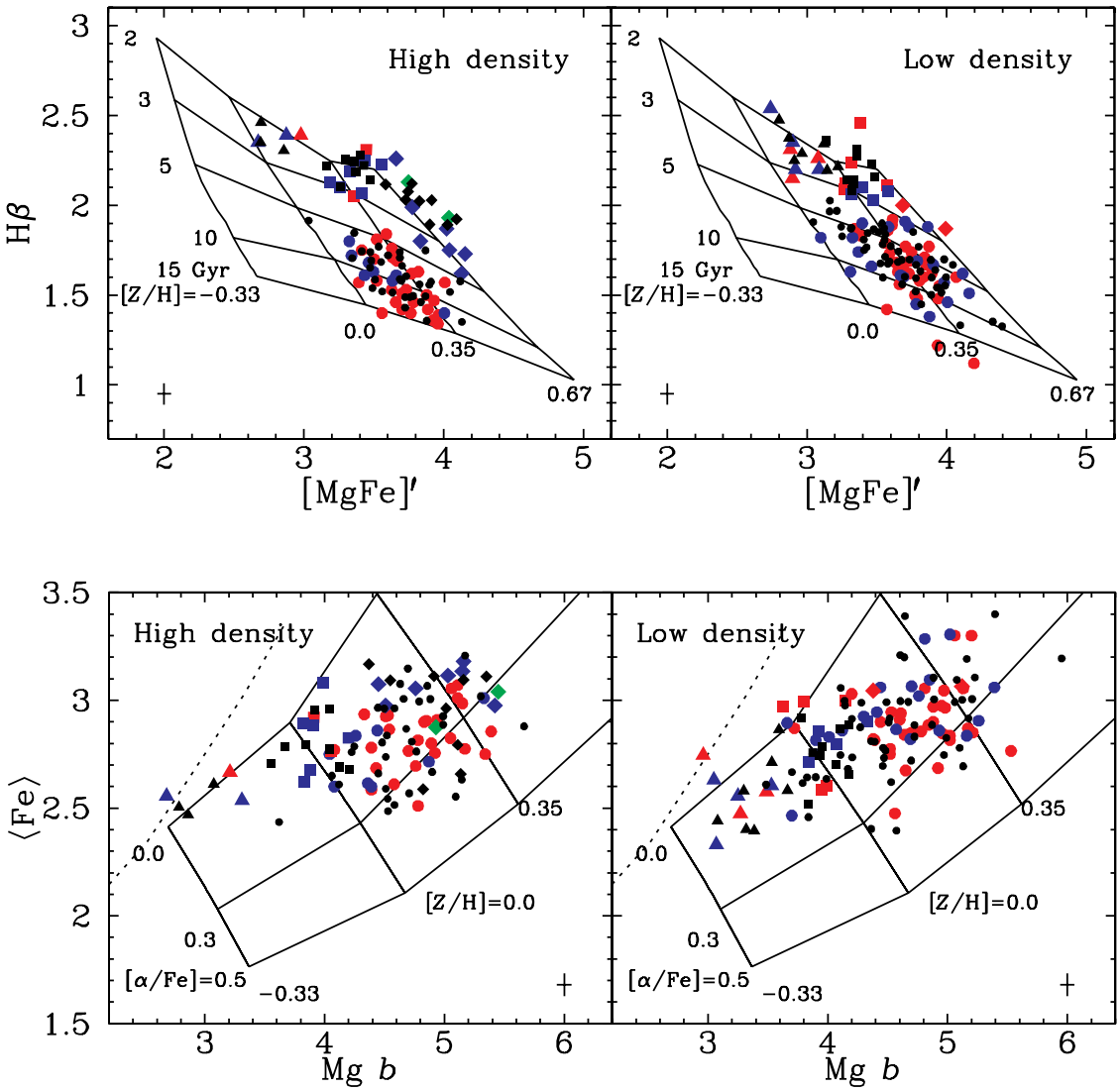

FIG. 4.—Lick indices $[\mathrm{MgFe}]'$ vs. Hβ (*top*) and Mg b vs. $\langle\mathrm{Fe}\rangle$ (*bottom*). Colored symbols represent the early-type galaxies analyzed in this paper (elliptical, *red*; S0, *blue*; cD, *green*), taken from González (1993), Beuing et al. (2002), and Mehlert et al. (2003), measured within $1/10r_e$. Median 1 σ error bars are shown. Black symbols represent Monte Carlo realizations. Circles assume linear relationships of age, metallicity, and α/Fe ratio with velocity dispersion (see eq. [1]). Triangles and squares represent simulations assuming 1.2 and 1.4 Gyr old subcomponents (10% and 20% in mass, respectively) on top of the above relationships, respectively. Diamonds represent realizations in which 70% of the galaxy's stellar populations is assumed to form around a look-back time of 2.5 Gyr (see Tables 1 and 2). Left and right panels show objects in high-and low-density environments, respectively. SSP models (TMB) with the metallicities $[Z/\mathrm{H}] = 0.0$, 0.35, and 0.67 are plotted for different ages $t = 2$, 3, 5, 10, and 15 Gyr at fixed α/Fe ratio ($[\alpha/\mathrm{Fe}] = 0$; *top*) and different α/Fe ratios $[\alpha/\mathrm{Fe}] = 0.0,\ 0.3,\ 0.5$ at fixed age ($t = 12$ Gyr; *bottom*) as indicated by the labels. Dotted lines in the bottom panels are models for $t = 2$ Gyr and $[\alpha/\mathrm{Fe}] = 0$.

means of the "age-metallicity" diagram (Fig. 4, *top*) we distinguish between four different categories, independent of the environment, as indicated by the symbol types: (1) V light–averaged ages older than ~5 Gyr (*circles*), (2) ages between 2 and 3 Gyr and metallicities $[Z/\mathrm{H}] \lesssim 0.35$ (*triangles*), (3) ages between 2 and 3 Gyr and metallicities $0.35 \lesssim [Z/\mathrm{H}] \lesssim 0.67$ (*squares*), and (4) ages between 2 and 5 Gyr and metallicities $[Z/\mathrm{H}] \gtrsim 0.67$ (*diamonds*).

Here we provide a short summary of how these categories are reproduced; they are described in detail in §§ 4.1–4.4. Category 1 contains intermediate-mass and massive galaxies [$120 \lesssim \sigma/(\mathrm{km\ s^{-1}}) \lesssim 320$] and can be reproduced by linear relationships between the stellar population parameters and $\log \sigma$. For simplicity we call this category "old population," since categories 2–4, unlike category 1, require two-component models with young subpopulations. Category 2 consists of *low-mass galaxies* [$50 \lesssim \sigma/(\mathrm{km\ s^{-1}}) \lesssim 130$] and is reproduced assuming a minor (10% in mass) young (~1.2 Gyr) subcomponent. Category 3 are *young intermediate-mass* galaxies [$110 \lesssim \sigma/(\mathrm{km\ s^{-1}}) \lesssim 230$] with a minor (20% in mass) young (~1.4 Gyr) component, while category 4 contains *young massive galaxies* [$190 \lesssim \sigma/(\mathrm{km\ s^{-1}}) \lesssim 360$] with a major (70% in mass) young (~2.5 Gyr) component. The data sample is well characterized by these four object classes and well reproduced by the Monte Carlo simulations. In the following section we discuss their characteristics in detail. They are summarized in Tables 1 and 2.

4.1. *Old Population (Circles)*

This subpopulation represents the major fraction of the present sample, namely, 60% and 70% in high- and low-density environments, respectively, containing both elliptical and lenticular galaxies. The objects display relatively well-defined relationships between absorption-line indices and central velocity dispersion, as shown in Figure 5 (*colored symbols*). Both

TABLE 1
Model Parameters

Parameter	Circles	Triangles	Squares	Diamonds
σ (km s^{-1})	120–320	50–130	110–230	190–360
$\log(M_*/M_\odot)$	10–12	<10	10–11	>11
First component	eq. (1)	eq. (1)	eq. (1)	eq. (1)
Second component	No	Yes	Yes	Yes
Mass (%)	...	10	20	70
Age (Gyr)	...	1.2	1.4	2.5
$[Z/H]$	...	$\sim$0.2	$\sim$0.8	$\sim$0.7
$[\alpha/Fe]$	...	~-0.06	$\sim$0.20	$\sim$0.34

Notes.—Stellar masses (row 2) are from eq. (2). The last five rows refer to the second component.

metallic indices Mg b and $\langle$Fe$\rangle$ correlate with velocity dispersion, which is well known for Mg b (e.g., Bender et al. 1993) and has also been recently established for $\langle$Fe$\rangle$ (Kuntschner et al. 2001; Caldwell et al. 2003; Bernardi et al. 2003). The Balmer index Hβ, instead, clearly tends to decrease with increasing σ (see also Kuntschner et al. 2001; Caldwell et al. 2003; Bernardi et al. 2003). Figure 5 shows that these relationships are essentially independent of the environment, except that the $\langle$Fe$\rangle$-σ relation seems somewhat flatter in low-density environments.

4.1.1. *Scaling Relations*

The black symbols in Figure 5 are the Monte Carlo realizations corresponding to the dominating "old" population (Fig. 4, *circles*). In these simulations we have assumed linear correlations of the parameters age, metallicity, and α/Fe ratio with $\log\sigma$. The dependencies that best fit all three indices as functions of velocity dispersion for objects in high-density environments are (quantities in brackets are the values derived for the low-density environment)

$$\begin{aligned}[\alpha/\mathrm{Fe}] &= -0.42(-0.42) + 0.28(0.28)\log\sigma,\\ [Z/\mathrm{H}] &= -1.06(-1.03) + 0.55(0.57)\log\sigma,\\ \log t/\mathrm{Gyr} &= 0.46(0.17) + 0.238(0.32)\log\sigma. \end{aligned} \quad (1)$$

The simulations take the observational errors (see Fig. 3) into account plus an intrinsic scatter $\Delta[\alpha/\mathrm{Fe}] = 0.05$ dex, $\Delta[Z/\mathrm{H}] = 0.08$ dex, and $\Delta t = 0.2t$ Gyr in high-density environments and $\Delta[\alpha/\mathrm{Fe}] = 0.07$ dex, $\Delta[Z/\mathrm{H}] = 0.10$ dex, and $\Delta t = 0.25t$ Gyr in low-density environments. The relationships with velocity dispersion including their scatter of the line indices are well reproduced. The relative contributions of the observational errors and the intrinsic scatter of the stellar population parameters to the overall spread in the data and simulations is discussed in more detail below.

Before doing so, we provide estimates of the stellar masses as a function of velocity dispersion. For this purpose we transform the ages and metallicities of equation (1) into stellar mass-to-light ratios with the help of stellar population models and use these to derive (via the Faber-Jackson relation; Faber & Jackson 1976) a relationship between stellar mass and velocity dispersion. We adopt the SSP models of Maraston (2004) for a Kroupa initial mass function (IMF; note that a Salpeter IMF yields M/L ratios, hence masses, that are higher by a factor of 1.6). The M/L ratios (and masses) derived in this way from the high- and low-density relationships vary by only 25% because the younger ages of the low-density objects are balanced by higher metallicities. In the following equation we therefore provide the resulting relationship between stellar mass M_* and $\log\sigma$ averaged over both environments,

$$\log M_* \approx 0.63 + 4.52\log\sigma. \quad (2)$$

This yields the following relations between the stellar population parameters and galaxy stellar mass:

$$\begin{aligned}[\alpha/\mathrm{Fe}] &= -0.459(-0.459) + 0.062(0.062)\log(M_*/M_\odot),\\ [Z/\mathrm{H}] &= -1.137(-1.109) + 0.1217(0.1261)\log(M_*/M_\odot),\\ \log t/\mathrm{Gyr} &= 0.427(0.125) + 0.053(0.071)\log(M_*/M_\odot). \end{aligned} \quad (3)$$

4.1.2. *Stellar Population Parameters*

Figure 6 shows velocity dispersion and stellar mass versus the stellar population parameters age, metallicity $[Z/\mathrm{H}]$, and $[\alpha/\mathrm{Fe}]$ ratio derived from the line indices shown in Figure 5. They are summarized in Table 3. Observational data are the colored symbols (see Fig. 2); the Monte Carlo realizations are shown as black circles. The lines indicate the linear relationships of the stellar population parameters with $\log\sigma$ used in the simulations (see eq. [1]). The residuals of the data and Monte Carlo simulations from these relationships are shown in Figure 7 (*gray and hatched histograms, respectively*). Note that the simulations take both

TABLE 2
Sample Parameters and Line Indices

Name (1)	Sigma (2)	Error (3)	Hβ (4)	Error (5)	Mg b (6)	Error (7)	$\langle$Fe$\rangle$ (8)	Error (9)	Type (10)	Environment (11)	Source (12)	Class (13)
NGC 0221	72.1	2.6	2.31	0.05	2.96	0.03	2.75	0.03	E	Low density	González	Triangles
NGC 0224	156.1	3.7	1.67	0.07	4.85	0.05	3.10	0.04	S0	Low density	González	Circles
NGC 0315	321.0	3.9	1.74	0.06	4.84	0.05	2.88	0.05	E	Low density	González	Circles
NGC 0507	262.2	6.4	1.73	0.09	4.52	0.11	2.78	0.10	E	Low density	González	Circles
NGC 0547	235.6	3.6	1.58	0.07	5.02	0.05	2.82	0.05	E	Low density	González	Circles
NGC 0584	193.2	2.8	2.08	0.05	4.33	0.04	2.90	0.03	S0	Low density	González	Squares
NGC 0636	160.3	2.9	1.89	0.04	4.20	0.04	3.03	0.04	E	Low density	González	Circles
NGC 0720	238.6	5.2	1.77	0.12	5.17	0.11	2.87	0.09	E	Low density	Gonzalez	Circles
NGC 0821	188.7	2.9	1.66	0.04	4.53	0.04	2.95	0.04	E	Low density	González	Circles
NGC 1453	286.5	3.5	1.60	0.06	4.95	0.05	2.98	0.05	E	Low density	González	Circles

Notes.—Table 2 is published in its entirety in the electronic edition of the *Astrophysical Journal*. A portion is shown here for guidance regarding its form and content. Cols. (3), (5), (7), and (9) give 1 σ errors. Sources for the data (col. [12]): González (1993), Beuing et al. (2002), Mehlert et al. (2003), and C. Mendes de Oliveira et al. (2005, in preparation). The last column indicates the classification shown by symbol type in Fig. 4.

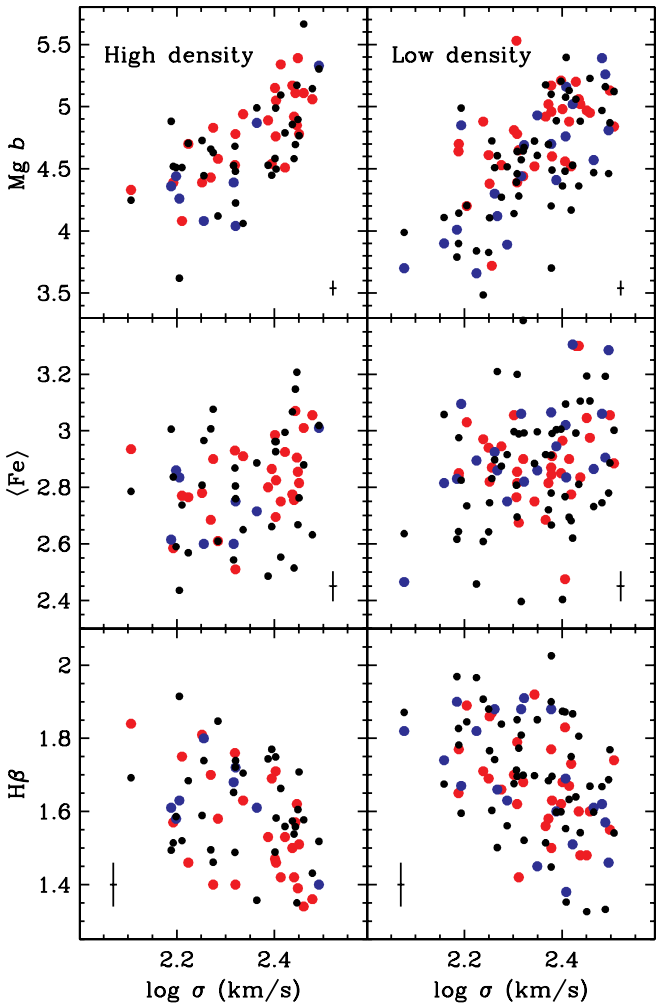

FIG. 5.—Absorption-line indices as functions of velocity dispersion (measured within $1/10r_e$) for the "old" subpopulation shown as circles in Fig. 4 (elliptical, *red*; S0, *blue*; cD, *green*; taken from González 1993; Beuing et al. 2002; Mehlert et al. 2003). Median 1 σ error bars are shown. The Monte Carlo realizations are shown by the black symbols. The latter take the observational errors (see Fig. 3) into account plus an intrinsic scatter $\Delta[\alpha/\mathrm{Fe}] = 0.05$ dex, $\Delta[Z/\mathrm{H}] = 0.08$ dex, and $\Delta t = 0.2t$ Gyr in high-density environments (*left*) and $\Delta[\alpha/\mathrm{Fe}] = 0.07$ dex, $\Delta[Z/\mathrm{H}] = 0.10$ dex, and $\Delta t = 0.25t$ Gyr in low-density environments (*right*).

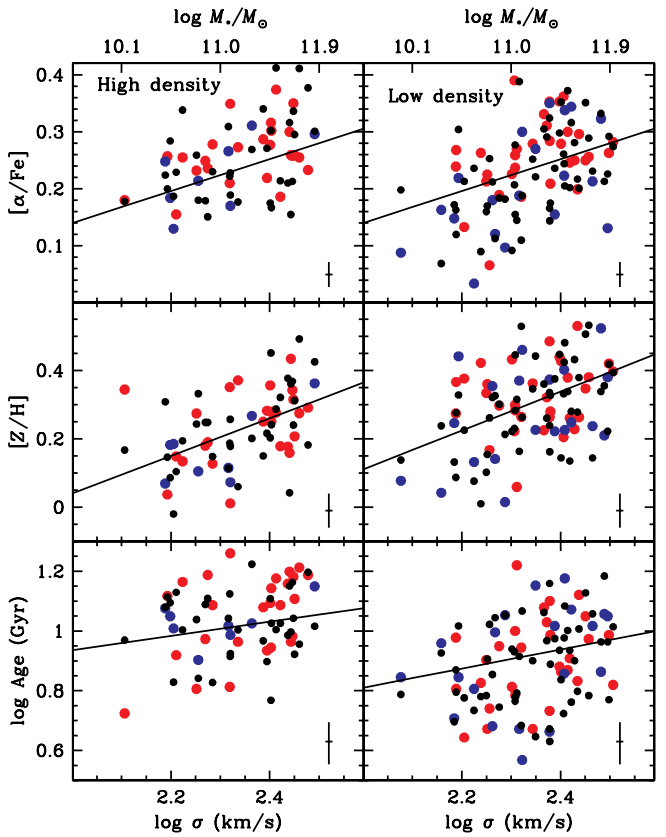

FIG. 6.—Stellar population parameters as a functions of velocity dispersion (measured within $1/10r_e$) and stellar mass (upper x-axis) for the old subpopulation (Figs. 4 and 5, *circles*). Ages and element abundances are derived with the $[\alpha/\mathrm{Fe}]$ enhanced SSP models described in § 2.2.1 from the indices Hβ, Mg b, and $\langle\mathrm{Fe}\rangle = (\mathrm{Fe5270} + \mathrm{Fe5335})/2$. Colored symbols are the values derived from the observational data (elliptical, *red*; S0, *blue*; cD, *green*); median 1 σ error bars are shown. The Monte Carlo realizations (*black circles*) take the observational errors (see Fig. 3) into account plus an intrinsic scatter $\Delta[\alpha/\mathrm{Fe}] = 0.05$ dex, $\Delta[Z/\mathrm{H}] = 0.08$ dex, and $\Delta t = 0.2t$ Gyr in high-density environments (*left*) and $\Delta[\alpha/\mathrm{Fe}] = 0.07$ dex, $\Delta[Z/\mathrm{H}] = 0.10$ dex, and $\Delta t = 0.25t$ Gyr in low-density environments (*right*). Typical error bars are given in the bottom right corners.

the observational errors plus an intrinsic scatter of the stellar population parameters at a given σ ($\Delta[\alpha/\mathrm{Fe}] = 0.05$ dex, $\Delta[Z/\mathrm{H}] = 0.08$ dex, and $\Delta t = 0.2t$ Gyr in high-density environments and $\Delta[\alpha/\mathrm{Fe}] = 0.07$ dex, $\Delta[Z/\mathrm{H}] = 0.10$ dex, and $\Delta t = 0.25t$ Gyr in low-density environments) into account. The red histograms are simulations without intrinsic scatter for comparison.

4.1.2.1. α/Fe

We find a very clear correlation between α/Fe ratio and $\log\sigma$ or stellar mass. The existence of this relation has already been anticipated qualitatively by a number of authors (e.g., Worthey et al. 1992; Fisher et al. 1995; Greggio 1997; Jørgensen 1999; Kuntschner 2000; Terlevich & Forbes 2002) and has only recently been confirmed quantitatively by means of stellar population models with variable element abundance ratios (Trager et al. 2000b; Proctor & Sansom 2002; Thomas et al. 2002; Mehlert et al. 2003). The observed scatter about the relation can only be reproduced assuming an intrinsic scatter in the $[\alpha/\mathrm{Fe}]$ ratio on the order of 0.05 dex, as shown by the hatched histograms

TABLE 3
RESULTS

Name	Age	Error	[Z/H]	Error	[α/Fe]	Error
NGC 0221.....	2.4	0.2	0.152	0.030	−0.025	0.013
NGC 0224.....	7.0	1.7	0.441	0.048	0.219	0.017
NGC 0315.....	6.6	1.4	0.397	0.038	0.282	0.019
NGC 0507.....	8.1	1.9	0.261	0.071	0.246	0.040
NGC 0547.....	10.7	1.7	0.321	0.049	0.311	0.020
NGC 0584.....	2.8	0.3	0.478	0.046	0.223	0.014
NGC 0636.....	4.4	0.6	0.376	0.028	0.133	0.013
NGC 0720.....	5.4	2.4	0.485	0.083	0.353	0.039
NGC 0821.....	8.9	1.2	0.297	0.036	0.189	0.015
NGC 1453.....	9.4	1.6	0.380	0.044	0.256	0.018

NOTES.—Table 3 is published in its entirety in the electronic edition of the *Astrophysical Journal*. A portion is shown here for guidance regarding its form and content. The stellar population parameters age, total metallicity [Z/H], and [α/Fe] abundance ratio are derived from Hβ, Mg b, and ⟨Fe⟩ (Table 2) using SSP models of Thomas et al. (2003a, 2004). Cols. (3), (5), and (7) give 1 σ errors. The latter are estimated via Monte Carlo simulations (see text).

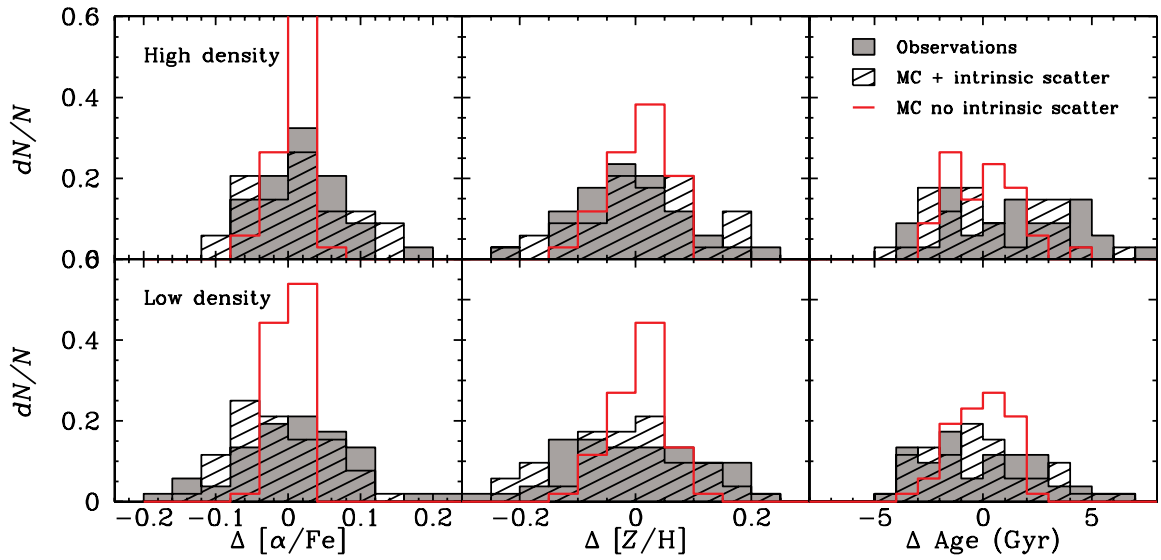

FIG. 7.—Residuals of the relations shown in Fig. 6 for the observationally derived data (*gray histograms*) and the simulations (*hatched histograms*). The latter take the observational errors (see Fig. 3) plus an intrinsic scatter $\Delta[\alpha/\mathrm{Fe}] = 0.05$ dex, $\Delta[Z/\mathrm{H}] = 0.08$ dex, and $\Delta t = 0.2t$ Gyr in high-density environments (*top*) and $\Delta[\alpha/\mathrm{Fe}] = 0.07$ dex, $\Delta[Z/\mathrm{H}] = 0.10$ dex, and $\Delta t = 0.25t$ Gyr in low-density environments (*bottom*) into account. The red histograms show the residuals of simulations without intrinsic scatter of the stellar population parameters.

in Figure 7. In the simulations without intrinsic scatter (Fig. 7, *red histograms*), the scatter in α/Fe is significantly smaller than the observed distribution.

Most interestingly, as already shown in Thomas et al. (2002), the α/Fe–σ relation (and its scatter) of early-type galaxies is independent of the environmental density (see also eq. [1]). This reinforces and extends the results of the studies by Jørgensen et al. (1995) and Terlevich & Forbes (2002), which are based on stellar population models tied to solar element ratios. Curiously, early-type galaxies in low-density environments seem to exhibit stronger CN absorption features than those in high-density environments (Sanchez-Blazquez et al. 2003). Since a significant fraction of C and N comes from intermediate-mass stars in the mass range $5 \lesssim M/M_{\odot} \lesssim 8$ (Renzini & Voli 1981), this points toward about 10^8 yr longer formation timescales in low-density environments. A delay well above this value can certainly be excluded, since the α/Fe ratio is independent of the environment. Hence, if true, the above result means that there must be an amazingly high degree of fine tuning in the formation timescales of early-type galaxies as a function of environmental density.

4.1.2.2. Z/H

Besides α/Fe, total metallicity Z/H also correlates with σ; hence, more massive early-type galaxies are also more metal-rich (see also Greggio 1997). This result is sensible in terms of chemical evolution, since the deeper potential well of massive objects hampers the development of a galactic wind, which leads to a more complete chemical processing to higher element abundances (e.g., Arimoto & Yoshii 1987; Matteucci 1994; Edmunds 1990). The observational scatter is best reproduced assuming about 0.1 dex of intrinsic scatter in total metallicity at a given velocity dispersion (Fig. 7, *hatched histograms*). Different from the α/Fe ratio, however, simulations without intrinsic scatter still provide a reasonable representation of the data (Fig. 7, *red histograms*).

Unlike for the α/Fe ratio, we detect a slight impact of the environmental density in the sense that galaxies in low-density environments appear about 0.05–0.1 dex more metal-rich than their counterparts in high-density environments (see also eq. [1]). This implies that galaxies in high-density environments seem to be more efficient in ejecting interstellar material in galactic winds, which might be caused by galaxy interactions and/or gas stripping processes.

4.1.2.3. Age

As noted in previous studies (Trager et al. 2000b; Kuntschner et al. 2001; Terlevich & Forbes 2002), age seems to be the weakest variable among early-type galaxies; the data show no significant trend between age and velocity dispersion. However, it has also been shown by Kuntschner et al. (2001) that correlated errors of age and metallicity tend to dilute a correlation between age and metallicity because a slight overestimation of Z/H leads to an underestimation of the age and vice versa. In Figure 6 we show that the observational data are best reproduced by a relatively flat but significant correlation between age and velocity dispersion (see solid lines and eq. [1]), in agreement with previous studies (Proctor & Sansom 2002; Proctor et al. 2004a, 2004b). The scatter of the observationally derived age (and of the Balmer index Hβ; see Fig. 5) is relatively well reproduced by the simulations without any intrinsic scatter (Fig. 7, *red histograms*). A scatter of the order of 20% at a given σ improves the fit, as shown by the hatched histograms in Figure 7.

To conclude, the mean age of early-type galaxies is weakly correlated with galaxy mass with about 20% intrinsic scatter. From this antihierarchical relationship we infer that the stellar populations of more massive early-type galaxies have formed earlier, which is further supported by their high α/Fe ratios.

Unlike in the case of the α/Fe ratio and total metallicity, we find a significant difference between the ages of galaxies in high- and low-density environments. There is a clear offset, indicating that the stellar populations of early-type galaxies in low-density environments are on average about 2 Gyr younger, in agreement with previous results (Trager et al. 2000b; Poggianti et al. 2001b; Kuntschner et al. 2002; Terlevich & Forbes 2002; Caldwell et al. 2003; Proctor et al. 2004b). This relative age difference caused by environmental effects is in very good agreement with the predictions from semianalytic models of galaxy formation (Kauffmann & Charlot 1998).

4.2. *Low-Mass Galaxies (Triangles)*

The objects of the low-mass tail of the velocity dispersion distribution (Fig. 1) with stellar masses $M_* < 10^{10}\ M_\odot$ (eq. [2]) all exhibit relatively high Balmer indices, indicating light-averaged ages between 2 and 3 Gyr (Fig. 4, *triangles*). We recover these objects with two-component composite stellar population models based on the old population (Fig. 4, *circles*), the properties of which are specified in equation (1). Extrapolation to the appropriate σ yields ages between 6 and 8 Gyr for the base old population. The average ages of the low-mass objects in both environments are then matched by contaminating this base old population with a 10% contribution (in mass) of a young ($\sim$1.2 Gyr) population (see Fig. 4, *filled triangles*). As mentioned earlier, this is certainly not a unique solution, since the contribution in mass and the look-back time of the star formation event are highly degenerate and therefore only poorly constrained. Alternatively, the addition of a major young component contributing 70% in mass with an age of 2 Gyr also reproduces the observed line indices. We can conclude, however, that relatively recent star formation in low-mass early-type galaxies is required to explain the observational data (see also Trager et al. 2000b).

The model with the minor young component gets some support from the α/Fe ratios. Figure 4 (*bottom*) shows that the Mg and Fe indices are also well reproduced by assuming that the young component is 0.2 dex less α/Fe enhanced than the base old population. This clearly favors the option of a young component over the possible presence of old blue horizontal branch stars as an explanation for the relatively strong Balmer absorption observed in low-mass galaxies. The metal indices of the objects are relatively weak; we needed to assume the young component to be about 0.2 dex more metal-rich than the base old population.

4.3. *Young Intermediate-Mass Galaxies (Squares)*

This subpopulation of objects with velocity dispersions between 110 and 230 km s^{-1}, hence $7 \times 10^9 \lesssim M_*/M_\odot \lesssim 2 \times 10^{11}$ (see eq. [2]), represents a minor fraction of the whole sample, namely, $\sim$14% containing both elliptical and lenticular types. There is no obvious dependence on environmental density and galaxy type. We consider the slight bias toward more lenticular galaxies in high-density environments (6 S0s of 8 early types in high density vs. 4 S0s of 9 early types in low density) as statistically not significant given the relatively small sample size.

The striking feature of these objects is their relatively strong Balmer line index, yielding light-average ages between 2 and 4 Gyr. To reproduce their Hβ indices, we model these galaxies with a two-component model, adding a minor young component as described in the previous paragraph. Different from low-mass galaxies, however, are the metallicities of the young subcomponent. To match the relatively strong [MgFe]$'$ index observed, extraordinarily high metallicities for the young component are required. The smaller the contribution (in mass) of the subcomponent is, the higher its metallicity needs to be. The avoidance of unplausibly high metallicities ($[Z/\mathrm{H}] \gtrsim 0.8$ dex) therefore sets a lower limit to the weight of the subpopulation. Metallicities below that limit are ensured if the young subpopulation contributes at least 20% in mass. For this lower limit, an age of 1.4 Gyr and metallicities around $[Z/\mathrm{H}] \sim 0.8$ dex are required to reproduce the observational data. An upper limit cannot be constrained. The high metallicity of the young component points toward a much higher effective yield during the formation of the young component in these intermediate-mass objects, compared to the low-mass objects discussed above. This means that chemical evolution and the buildup of metals is less efficient in low-mass objects, in agreement with the general picture that objects with shallower potential wells develop galactic winds more easily (e.g., Arimoto & Yoshii 1987; Matteucci 1994; Edmunds 1990; Chiosi & Carraro 2002).

Also different from the case of the low-mass galaxies, we had to assume the young population to have the same α/Fe ratio as the base old population in order to reproduce their Mg and Fe indices (Fig. 4, *bottom*; compare with dotted model lines for $t =$ 2 Gyr). This spoils the interpretation of the enhanced Balmer line strengths in terms of the presence of an intermediate-age stellar population. The separation in age between the old and young components amounts to several billion years, plenty of time for Type Ia supernovae to enrich the interstellar medium with iron. Forming out of this Fe-enhanced material, it will be impossible for the young component to reach significantly supersolar α/Fe ratios. Even the self-enrichment of the young component from Type II supernovae during the burst is not sufficient to raise the average α/Fe ratio of the newly born stellar populations independent of the burst timescale, as shown in Thomas et al. (1999).

The interpretation of the observed strong Balmer line indices in terms of recent star formation could be recovered under the rather contrived assumption that the Type Ia supernova ejecta originating from stars of the base old population have been lost selectively in galactic winds before the formation of the young subpopulation. Alternatively, the latter must have formed with a stellar IMF significantly flatter than Salpeter. A flat IMF slope would naturally reproduce the very high metallicity of the young component derived here. On the other hand, compelling evidence for systematic variations of the IMF slope in starbursts has not been found thus far (Leitherer 1998).

However, we have to be cautious here. Relatively high α/Fe ratios are needed for the young subpopulation because in the models Mg *b* decreases significantly with decreasing age at the highest metallicity, and it is possible that the fitting functions are in error in this regime owing to bad input stellar data. On top of this, the extraordinarily high metallicities of the young subcomponent ($[Z/\mathrm{H}] \sim 0.8$) require extrapolation well above the highest metallicity model ($[Z/\mathrm{H}] = 0.67$), which makes the model indices very unreliable. The relatively low Mg *b* index of the model, which causes the need for the relatively high α/Fe ratio, might be an artifact of bad calibration. To conclude, lower values for the young subpopulation cannot be excluded, which rehabilitates the possibility of the presence of an intermediate-age population.

Alternatively, the strong Balmer lines might be the result of blue horizontal branch stars rather than a young population, which we discuss in detail below.

4.4. *Young Massive Galaxies (Diamonds)*

Finally, the diamonds in Figure 4 indicate a subclass of very massive early-type galaxies ($M_* > 10^{11}\ M_\odot$) that have strong Hβ and strong [MgFe]$'$ absorption indices, implying light-averaged ages between 2 and 5 Gyr, and very high metallicities of $[Z/\mathrm{H}] \gtrsim 0.67$ dex. From Figure 4 it can be seen that the occurrence of these objects is restricted to high-density environments. Moreover, they are only lenticular galaxies; no elliptical galaxies with such low average ages and high metallicities are found (see Fig. 4). The vast majority (80%) of all S0 galaxies with $\sigma > 200$ km s^{-1} in our sample and the two Coma cD galaxies belong to this object class (see also Kuntschner 2000; Poggianti et al. 2001b; Mehlert et al. 2003).

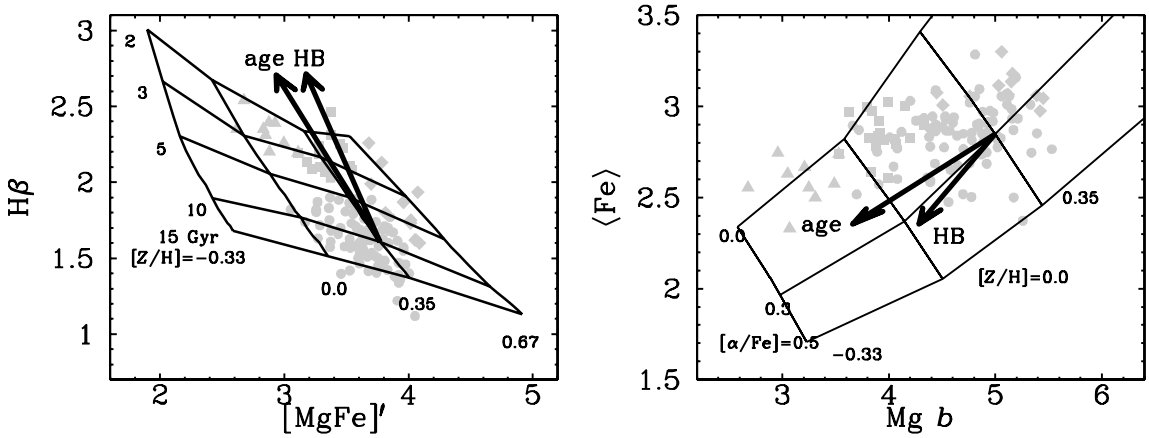

FIG. 8.—Comparison of the effects of age and blue horizontal branch on the absorption indices Hβ, Mg b, and $\langle$Fe$\rangle$. Symbols and model grid are as in Fig. 4. The arrows labeled "HB" show the index changes of a 10 Gyr population ($[Z/H] = 0.35$, $[\alpha/Fe] = 0.3$, red giant branch mass-loss parameter $\eta = 0.33$) when a blue horizontal branch $\eta = 0.55$ is considered. For comparison, the effect of reducing the age to 1.5 Gyr is indicated by the arrows labeled "age."

The metallicities are more than 0.2 dex above the average metallicity of the most massive objects in the old base population constrained by equation (1). Such a significant increase in average metallicity obviously cannot be obtained in a two-component model with only 10%–20% being a metal-rich subpopulation, unless unreasonable high metallicities above 10 times solar are assumed. We therefore have to increase the weight of the young population. The filled diamonds shown in Figure 4 are models in which the old base population is "perturbed" with a 2.5 Gyr young population with metallicities as high as $[Z/H] \sim 0.7$ dex contributing 70% in mass. Lower metallicities can be adopted only under the assumption that an even larger fraction of the stellar populations belongs to the second component.

Interestingly, as in the previous case these objects have very high α/Fe ratios. For the young component we need to adopt α/Fe ratios as they are given by equation (1); hence, $[\alpha/Fe] > 0.2$ for $\sigma > 200$ km s^{-1}. This fits well into the picture that the young average ages are not the result of minor recent star formation but rather the consequence of a recent very massive star formation event at a redshift around $z = 0.3$ forming the majority of the galaxy's stellar populations on a short timescale. This would imply that massive S0s and cD galaxies in clusters form very recently, while elliptical galaxies of comparable mass contain only old stellar populations. This explanation seems contrived, and it remains to be seen whether it can be understood in the framework of galaxy formation models.

4.5. *Blue Horizontal Branch Stars at High Metallicities*

Alternatively, the strong Hβ indices discussed above might be caused by the presence of metal-rich, blue horizontal branch stars (see § 1). Such blue horizontal branch stars may originate from either a metal-poor subpopulation as discussed in Maraston & Thomas (2000) or metal-rich populations with blue horizontal branch morphologies due to enhanced mass loss along the red giant branch evolutionary phase. Here we consider this latter option.

4.5.1. *The Origin of Blue Horizontal Branches*

The mass loss along the red giant branch can be theoretically understood as stellar winds being produced by the acoustic flux generated by the superadiabatic convection in the outer convective zone of the red giant (Fusi-Pecci & Renzini 1975). The fraction of acoustic energy that is used to remove the stellar envelope is not known from physically motivated first principles. An alternative is the empirical determination of the mass-loss rate, which has been done by Reimers (1975) studying the behavior of the circumstellar calcium K line in a large number of red giants and supergiants. The normalization of the resulting formula, however, suffers from very large uncertainties.

Fusi-Pecci & Renzini (1976) combined the two approaches and introduced an efficiency factor η for Reimers' formula. They calibrated the mass-loss rate with observational constraints such as the horizontal branch morphology (Rood 1973), the limiting initial mass for carbon ignition ($\sim 4\,M_\odot$ for the Hyades; van den Heuvel 1975), and finally the solar mass-loss rate. An efficiency $\eta \approx 0.33$ turned out to be the most appropriate choice. This value is adopted in the models of Maraston (1998, 2004). Note that the observational uncertainties in Reimer's formula allow this efficiency factor to lie in the range $0.3 \lesssim \eta \lesssim 3$. The problem is that the calibration has been carried out at subsolar metallicity, and deviations from this canonical value, in particular at higher metallicities, cannot be excluded (Greggio & Renzini 1990).

4.5.2. *Effect on the Line Indices*

The models of TMB are based on Maraston (1998, 2004) and thus rely on the calibrated value $\eta = 0.33$. Here we additionally compute models with the slightly larger efficiency factor $\eta = 0.55$, which is well within the range of uncertainty allowed by the Reimers formula. These models have bluer horizontal branch morphologies and therefore predict significantly stronger Balmer indices and slightly weaker metallic indices. This is shown in Figure 8 (*left*) by the arrow labeled "HB" for a 10 Gyr old population. The arrow labeled "age" shows the location of a model with age $t = 1.5$ Gyr, which yields the same Hβ value, for comparison. The steeper slope of the HB model illustrates the weaker sensitivity of the metallic line indices to horizontal branch morphology than to age. The relative effect of Mg b and $\langle$Fe$\rangle$ is shown in Figure 8 (*right*). Relative to $\langle$Fe$\rangle$, the Mg b index responds more strongly to a decrease of age than to a blueing of the horizontal branch. As a consequence, the slope of the HB model is also steeper in the Mg b–$\langle$Fe$\rangle$ diagram. Note that the slope is comparable to that of the model varying metallicity at a constant α/Fe ratio and age.

4.5.3. *Two-Component Model*

These results will mainly affect the age determination. To test this, we have constructed a two-component model in which the base old population is contaminated with 50% of an old metal-rich

population with blue horizontal branch stars. The location of both the squares and the diamonds in Figure 4 is reached by these models without invoking the presence of intermediate-age populations. We had to assume the metallicity of the second component to be about 0.2–0.4 dex higher than the average of the base population, while the α/Fe ratio needs to be about 0.1 dex lower. Hence, the blue HB option requires the assumption that preferentially the metal-rich stars in a composite stellar population develop blue horizontal branches. The slightly lower α/Fe ratios would fit into this picture, since the most metal-rich populations must have formed latest and should therefore be least α/Fe enhanced.

4.5.4. *Young versus Blue Horizontal Branch*

To conclude, neither option—intermediate-age population nor blue horizontal branch—can be excluded; further observational constraints to distinguish the two alternative explanations are required. If intermediate-age populations are present in these galaxies, they should be detectable by their very red near-infrared colors, because of the major contribution to the bolometric from asymptotic giant branch stars at ages between 0.5 and 2 Gyr (Maraston 1998, 2004, 2005; Maraston et al. 2001; Silva & Bothun 1998).

Unambiguous indicators of blue horizontal branches, instead, still need to be found. The Ca II index defined by Rose (1984), even though promising, does not solve the problem because it is still degenerate between gravity and metallicity effects. Schiavon et al. (2004) show that in metal-poor globular clusters the higher order Balmer line index Hδ_F is more sensitive to the presence of blue horizontal branches than Hβ. Hence, the index ratio Hδ_F/Hβ may be a tool to break the degeneracy between age and horizontal branch morphology. It is not clear, however, whether this effect is still present at solar metallicities and above, which are relevant to massive galaxies. Moreover, in Thomas et al. (2004) we show that at such high metallicities the Hδ_F/Hβ index ratio becomes very sensitive to the α/Fe ratio in the sense that Hδ_F/Hβ increases with α/Fe. If blue horizontal branches ought to be detected in early-type galaxies by means of the Hδ_F/Hβ ratio, the dependence on α/Fe certainly has to be taken into account. It will be interesting to make these checks for the galaxy sample discussed here. Such an analysis will be the subject of a future study.

5. THE ORIGIN OF THE Mg-σ RELATION

The correlations of the stellar population parameters age, total metallicity, and α/Fe ratio with central velocity dispersion shown in Figure 6 and equation (1) allow us to constrain the origin of the well-known Mg-σ relation (Fig. 5, *top*). We recall that the correlations found here suggest that all three parameters correlate with σ and hence support the Mg-σ relationship.

Figure 9 shows the observed Mg b–σ relation of the whole sample, high- and low-density environments combined. It can be verified from Figure 5 that the environment has a negligible effect on the Mg-σ relation, in agreement with previous findings based on much larger samples (Bernardi et al. 1998; Colless et al. 1999; Worthey & Collobert 2003). Circles are the old population representing the major fraction of the sample, while triangles, squares, and diamonds are the "young outliers" discussed in the previous section (see also Fig. 4). Red and blue symbols are elliptical and lenticular galaxies, respectively. Green symbols are cD galaxies. The black symbols are the Monte Carlo realizations. The solid line is the Mg b–σ relation that results from the relationships given in equation (1) (averaging over both environments). The short-dashed line shows the resulting Mg b–σ relation if only age is assumed to be the driving parameter adopting equation (1). The dependencies of both total metallicity and α/Fe ratio with σ are suppressed. The long-dashed line demonstrates the effect of additionally adding the dependence on α/Fe ratio from equation (1).

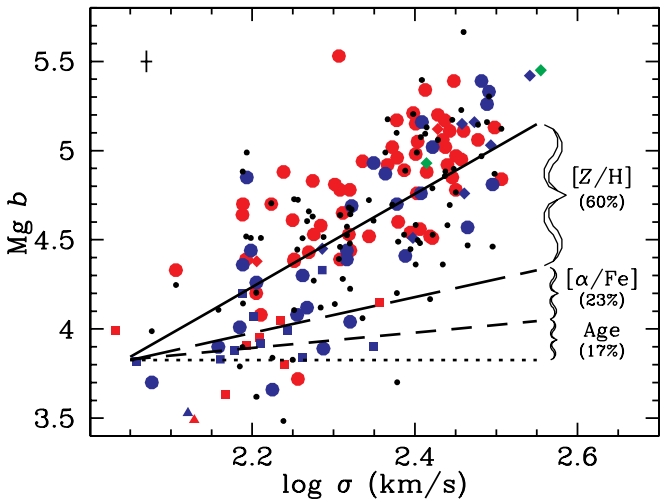

FIG. 9.—Mg b–σ relation of the whole sample high-density and low-density environments combined. Colored symbols are observational data (elliptical, *red*; S0, *blue*; cD, *green*); median 1 σ error bars are shown. Black symbols represent Monte Carlo simulations (symbol types as in Fig. 4). The solid line shows the Mg b–σ relation resulting from the relationships given in eq. (1) averaging over high-and low-density environments. The short-dashed line shows the resulting Mg b–σ relation if only age is assumed to be the driving parameter adopting eq. (1). The long-dashed line demonstrates the effect of additionally adding the dependence on α/Fe ratio from eq. (1).

It can be seen that total metallicity has by far the largest share (60%) in shaping the relation, followed by the α/Fe ratio contributing only 23% to the observed slope. The contribution from age is about 17% and hence is the smallest but comparable to that of α/Fe. We emphasize that these numbers do not vary significantly with environmental density. As can be inferred from Figures 5 and 6, the scatter of the Mg b–σ relation among the old population (*circles*) results from intrinsic scatter in all three stellar population parameters. The $\langle$Fe$\rangle$-σ relation is much shallower (see Fig. 5) because the increasing α/Fe ratio with σ diminishes the $\langle$Fe$\rangle$ index, largely compensating for the increase due to increasing metallicity (see also Mehlert et al. 2003).

This result fits very well with the fact that the color-magnitude relation also appears to be driven by metallicity rather than age (Kodama & Arimoto 1997; Stanford et al. 1998; Terlevich et al. 1999; Vazdekis et al. 2001; Merluzzi et al. 2003), even though the effect of the α/Fe ratio variations on colors is still not very well understood (Thomas & Maraston 2003).

Finally, we briefly examine the location of the young outliers of Figure 4 (*triangles*, *squares*, *and diamonds*). The low-mass and intermediate-mass objects with young light-averaged ages (*triangles and squares*) are clearly off the relation and exhibit systematically lower index values (by $\sim$0.5 Å) at a given σ. Their slightly larger light-averaged metallicities (see Fig. 4) obviously do not suffice to bring them back onto the relationship. The case of the class of massive, apparently young Coma Cluster lenticular galaxies (*diamonds*) is different. Their extremely high light-averaged metallicities compensate totally for the decrease in Mg b caused by the young light-averaged ages. As far as the Mg b–σ relation is concerned, these objects are indistinguishable from the main body of the sample.

6. FORMATION EPOCHS

The relations shown in Figure 6 (see also eqs. [1] and [3]) can be used to constrain the epochs of the main star formation episodes and the star formation timescales for early-type galaxies as a function of their mass and environmental densities. It should be emphasized that the majority of the objects in the present sample obey these relationships. Only 15% of the sample (Fig. 4, *squares*) require a 20% contribution from intermediate-age populations on top of the base old population described by equation (1), and a further 9% (*diamonds*) are best modeled assuming 70% young populations. The young low-mass galaxies (Fig. 4, *triangles*) do not play a significant role in the total mass budget of early-type galaxies, the latter being dominated by L^* galaxies with $M_* \sim 10^{11}\ M_\odot$ situated at the turnover of the luminosity (mass) function (Bell et al. 2003; Baldry et al. 2004). This implies that about 90% of the total stellar mass hosted by early-type galaxies is well represented by the relationships given in equation (1).

6.1. *Relating Timescale and* α/Fe *Ratio*

The key point of this analysis is that the α/Fe ratio lifts the degeneracy between formation epoch and formation timescale. This is done by relating the observationally derived luminosity-averaged α/Fe ratios of the stellar populations with the timescales of their formation. For this purpose we simulate the formation and chemical evolution of a set of toy galaxies assuming various star formation histories characterized by different timescales, similar to the exercise presented in Thomas et al. (1999).

We start with a gas cloud of primordial chemical composition. By imposing a star formation rate as a function of time, which is given by the specific star formation history assumed, we let the gas cloud form stars. These stars enrich the gas of the cloud (the interstellar medium) with heavy elements produced mainly in supernova explosions. For the aim of this paper we follow the chemical enrichment of α and Fe peak elements. A key point is that we take the delayed enrichment of Fe from Type Ia supernovae into account using the prescription of Greggio & Renzini (1983; see Thomas et al. 1998 for more details). Stellar populations successively form out of more and more chemically enriched gas, resulting in the buildup of a composite stellar population. Every generation of stars in this composite will have the chemical composition, and hence α/Fe ratio, of the gas out of which it had formed. We examine this population 12 Gyr after the formation of the first stellar generation and calculate its V light–averaged [α/Fe] ratio, which corresponds to the quantity observationally derived in this study. The weight in V luminosity of the single stellar populations as a function of their ages is adopted from the M/L ratios of Maraston (2005). The IMF slope is kept fixed to Salpeter. As in Thomas et al. (1999), the simulations are carried out assuming a closed box, which implies that selective mass loss is assumed not to occur and thus not to affect the α/Fe ratio.

The star formation histories in the different runs are chosen to be Gaussians of various widths Δt (FWHM). We find the following linear relationship between α/Fe ratio and $\log \Delta t$:

$$[\alpha/\mathrm{Fe}] \approx \frac{1}{5} - \frac{1}{6} \log \Delta t. \quad (4)$$

The equation reflects what has already been shown in Thomas et al. (1999), namely, that a ratio $[\alpha/\mathrm{Fe}] = 0.2$ of a composite stellar population requires formation timescales $\Delta t \lesssim 1$ Gyr. The larger Δt, the lower is the final α/Fe ratio of the stellar population because of the late enrichment of Fe from Type Ia supernovae. Star formation extended over the Hubble time yields an α/Fe close to solar. We note that this link between α/Fe ratio and star formation timescale is in very good agreement with the more detailed chemical evolution simulations of Pipino & Matteucci (2004).

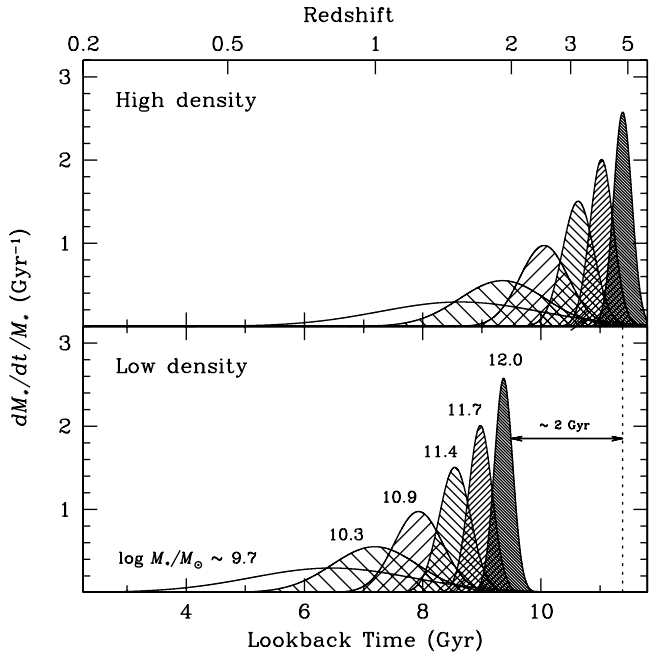

FIG. 10.—Star formation histories of early-type galaxies as a function of their stellar masses M_* (see labels). The stellar masses M_* correspond to the velocity dispersions $\sigma = 100$, 140, 190, 240, 280, and 320 km s^{-1} (see eq. [2]). The star formation histories are derived from the mean ages and [α/Fe] ratios shown in Fig. 6 and eqs. (1) (or [3]) and (4). Redshifts assume $\Omega_m = 0.3$, $\Omega_\Lambda = 0.7$, and $H_0 = 75$ km s^{-1} Mpc^{-1} (Spergel et al. 2003). The dotted line marks the average age of a high-density object with $M_* = 10^{11}\ M_\odot$ ($\sigma = 320$ km s^{-1}) for comparison.

The combination of equations (1) and (3) with equation (4) then yields correlations of Δt with σ and mass for early-type galaxies valid in both high and low environmental densities:

$$\log \Delta t \approx 3.44 - 1.68 \log \sigma \approx 3.67 - 0.37 \log (M_*/M_\odot). \quad (5)$$

Equations (1) and (3) further give the light-average ages as a function of σ, constraining the epoch at which the object has formed.

6.2. *The Star Formation Histories*

The resulting star formation histories for various galaxy masses and velocity dispersions are shown in Figure 10. The x-axis is look-back time; the upper x-axis gives the corresponding redshifts assuming $\Omega_m = 0.3$, $\Omega_\Lambda = 0.7$, and $H_0 = 75$ km s^{-1} Mpc^{-1} (Spergel et al. 2003). The top and bottom panels show the results for dense and loose environments, respectively.

It should be kept in mind that Figure 10 is based on average ages and α/Fe ratios at a given mass. As discussed in § 4, the data require a scatter in α/Fe ratio of the order of 0.05–0.07 dex (see Fig. 7), which translates into a spread in star formation timescale of about a factor of 2. The observed spread in average age is consistent with a scatter of about 20%–25% (see Fig. 7). For a cluster early-type galaxy with stellar mass $M_* \sim 5 \times 10^{11}\ M_\odot$ ($\sigma = 280$ km s^{-1}), for instance, this implies a spread about the

typical formation redshift at $z \sim 3$ between $z \sim 2$ and 5. The blurring caused by these effects should be kept in mind for the interpretation of the diagrams in Figure 10, which are meant to be schematic illustrations of the mean formation epochs.

6.3. *Dependence on Galaxy Mass*

The plots summarize what has already been discussed in the previous sections. The more massive the galaxy is, the faster and earlier form its stellar populations. Indeed, Pipino & Matteucci (2004) show that the observed relation between α/Fe and σ can be best reproduced by a model in which gas accretion and star formation timescales decrease with increasing galaxy mass. Only low-mass galaxies exhibit significant star formation at redshifts below $z \lesssim 1$, as also concluded by Brinchmann & Ellis (2000) and more recently by De Lucia et al. (2004) and Jimenez et al. (2005) based on Sloan Digital Sky Survey data. These results are also in very good agreement with the star formation histories found by Gavazzi et al. (2002) based on spectrophotometric data. Interestingly, the link between star formation histories and galaxy mass shown in Figure 10 agrees well with the predictions from *N*-body–tree–smoothed particle hydrodynamics simulations by Chiosi & Carraro (2002), which are based on a monolithic collapse inside a dark matter halo rather than hierarchical structure formation.

Note that we have assumed continuous star formation in order to keep the number of free parameters low. The principal aim of this exercise is to illustrate the typical timescale of the star formation histories in galaxies as a function of their masses. In reality, star formation in individual objects will be less smooth and will be shaped by several bursty star formation episodes (see Chiosi & Carraro 2002). The functions of Figure 10 thus have to be understood as integrals at a given velocity dispersion over bursty star formation histories. In particular, the extended star formation histories of the low-mass objects might rather be understood in terms of episodically returning star-forming bursts, similar to what is found in dwarf galaxies of the Local Group (Mateo 1998).

In massive systems, the burst might well be triggered by merger events. Indeed, a considerable fraction of massive elliptical galaxies have kinematically decoupled cores (Bender 1988; Franx & Illingworth 1988), the presence of which requires the merger to be accompanied by dissipational processes and star formation. Interestingly, for a number of elliptical galaxies with kinematically decoupled cores, it has been found that their stellar populations are homogeneously old and α/Fe enhanced (Surma & Bender 1995; Mehlert et al. 1998; Davies et al. 2001), indicating that the merger happened at early times, in agreement with the formation histories of Figure 10 (a counterexample is NGC 2865; Hau et al. 1999).

6.4. *Influence of the Environment*

The second main result is that galaxy formation appears delayed by $\sim$2 Gyr in low-density environments, confirming previous findings (Trager et al. 2000b; Poggianti et al. 2001b; Kuntschner et al. 2002; Terlevich & Forbes 2002; Caldwell et al. 2003; Proctor et al. 2004b). This is in agreement with studies of the field galaxy population at intermediate redshifts around $z \sim 1$ (van Dokkum et al. 2001; Treu et al. 2002; Gebhardt et al. 2003). While the formation of massive early-type galaxies in clusters sets in at redshifts around $z \sim 5$ and is completed (in terms of their stellar populations) at about $z \sim 2$, a considerable fraction of massive galaxy formation in low-density environments occurs at lower redshifts between $z \sim 1$ and 2. We recall here that the α/Fe–σ relation does not depend on environmental density. The timescale of star formation in an object is determined by its (final) mass rather than the environment. As a consequence, massive early-type galaxies in low-density environments form later but on timescales similar to those of their counterparts in high environmental densities, as illustrated in Figure 10.

7. DISCUSSION

7.1. *The Local Abundance Pattern at High Metallicities*

In a recent study, Proctor et al. (2004b) argue that the correlation of α/Fe with velocity dispersion is an "artefact of incomplete calibration (of the models) to the Lick system." The basis for their conclusion is the recent finding of Bensby et al. (2004) that the Milky Way disk stars with supersolar metallicities do not have solar but subsolar O/Fe ratios, O/Fe decreasing with increasing Fe/H (see also Pompéia et al. 2003; Allende Prieto et al. 2004). Stellar population models, being calibrated with these stars, are then likely to reflect subsolar O/Fe ratios at high metallicities. If the element oxygen is taken as representative for all α-elements, this would obviously lead to an overestimation of the O/Fe ratio (or α/Fe ratio) in stellar populations with supersolar metallicities such as early-type galaxies. Proctor et al. (2004b) show that the correction for this effect makes the α/Fe–σ relation disappear.

However, there is a further very important (and somewhat puzzling) point made by Bensby et al. (2004). All the other α-elements, Mg, Si, Al, Na, Ca, and Ti, do not show this pattern, but level off at a solar X/Fe ratio in stars with supersolar metallicities (Fuhrmann 1998; Bensby et al. 2003). Only the element oxygen (and maybe also carbon; Thorén et al. 2004) deviates from this homogeneous behavior. This differential pattern between oxygen and the other α-elements cannot be neglected in models taking the local abundance pattern at high metallicities into account. This is particularly important in the context of this work, as the α/Fe ratios presented here are derived from the absorption-line indices Mg *b* and $\langle$Fe$\rangle$, which are sensitive mostly to the elements Fe and Mg but *not* O (Tripicco & Bell 1995; Korn et al. 2004).

We investigated this issue by constructing two additional flavors of stellar population models that account for this local abundance pattern at high metallicities. The first model takes oxygen as representative of all α-elements (as in Proctor et al. 2004b); in the second model oxygen is detached from the rest of the α-elements as discussed above. The resulting models in the index-index planes and the stellar population parameters derived with these models are shown in Figures 11 and 12 (equivalent to Fig. 2) and Figures 13 and 14 (equivalent to Fig. 6). The results are discussed in detail in the Appendix.

To summarize, we reproduce the result of Proctor et al. (2004b) with the model in which oxygen and α-elements are not separated. The α/Fe–σ relation disappears, the *Z*/H–σ relation becomes tighter, while the ages remain unchanged. When oxygen is detached from the other α-elements as suggested by observations, the picture is entirely different, as explained in detail in Appendix B. The correction for the local abundance pattern has no significant impact on the model when the nonsolar O/Mg ratios of metal-rich stars in the solar neighborhood are taken into account. The model basically moves back to its original position. As a consequence, the stellar population parameters derived with this model are in excellent agreement with the ones presented in this work (see Fig. 14).

To conclude, the results of this paper are robust against the correction for the local abundance pattern at high metallicities.

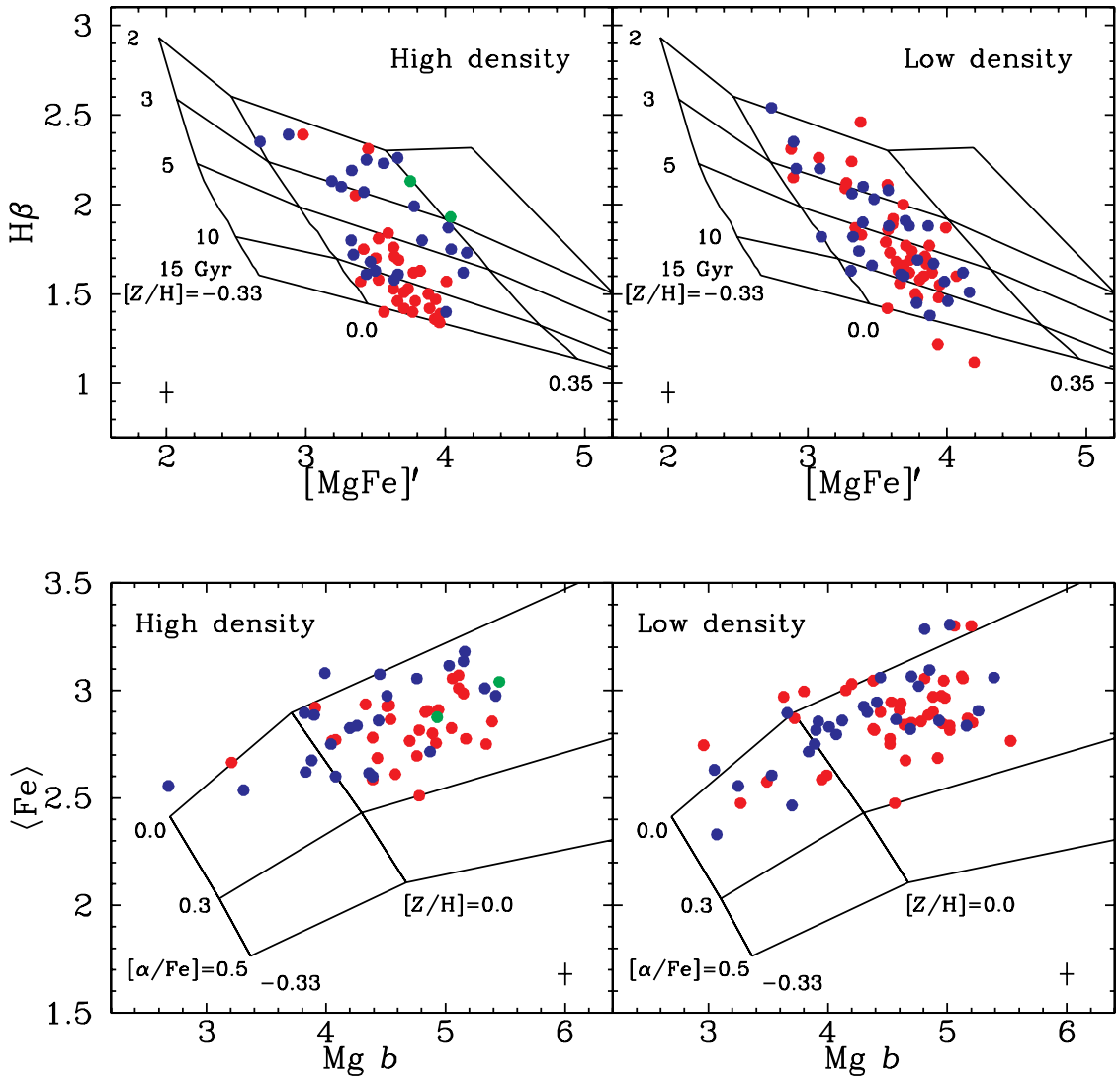

FIG. 11.—Same as Fig. 2, but the models are corrected for the decrease of O/Fe with increasing metallicity at supersolar metallicity in the solar neighborhood assuming oxygen and the other α-elements being lumped together.

In particular, the α/Fe–σ relation found here is real and is not caused by calibration artifacts. What remains to be understood is the discrepancy between oxygen and the other α-elements in the metal-rich stars of the solar neighborhood.

As discussed in Bensby et al. (2004), a possible explanation is that Type Ia supernovae do produce a significant amount of magnesium, which keeps the Mg/Fe ratio solar, while O/Fe decreases with increasing metallicity. This would also fit the slightly higher O/Fe than Mg/Fe ratios in metal-poor stars of the Milky Way (Bensby et al. 2004). In this case, the standard model for Type Ia nucleosynthesis (the so-called W7 model; Nomoto et al. 1984) needs to be revised. This leads to speculation that the importance of Type Ia enrichment may increase steadily with atomic number of the element up to Fe and Ni. If this is the case, the higher the atomic number of the element, the flatter should be the X/Fe–Fe/H relation in the Milky Way. In particular, elements with high atomic number should have lower X/Fe ratios in the metal-poor halo stars, which has not been confirmed in the review of McWilliam (1997). Maybe new data sets will revolutionize this statement. If true, the low Ca/Mg ratios of early-type galaxies (e.g., Thomas et al. 2003b) would naturally be explained in terms of delayed Type Ia supernova enrichment (Pipino & Matteucci 2004).

The relevant inference for this paper would be that the formation timescales discussed in § 6 (eq. [4]) are underestimated. A detailed investigation and quantification of this effect goes far beyond the scope of this paper and, in particular, cannot be performed in a straightforward way because the appropriate Type Ia nucleosynthesis calculations are not available. Note, however, that the high α/Fe ratios derived here for massive galaxies, suggesting short star formation timescales, are coupled with high average ages, which further reinforces this interpretation. The results of this work suggest star formation timescales as short as only a few times 10^8 yr in the most massive early-type galaxies with $M_* \sim 10^{12}\ M_\odot$. It would certainly be desirable if such extreme timescales were slightly relaxed by an additional contribution from Type Ia supernovae to the enrichment of the heavier α-elements. It should be emphasized that a fundamental conclusion of this paper is that low-mass galaxies have more extended formation timescales. This purely differential result is not affected if Type Ia supernovae represent an additional source of α-elements.

7.2. *Comparison with Early Results*

The findings discussed in this paper are supported by a number of pieces of evidence from the tightness and the redshift

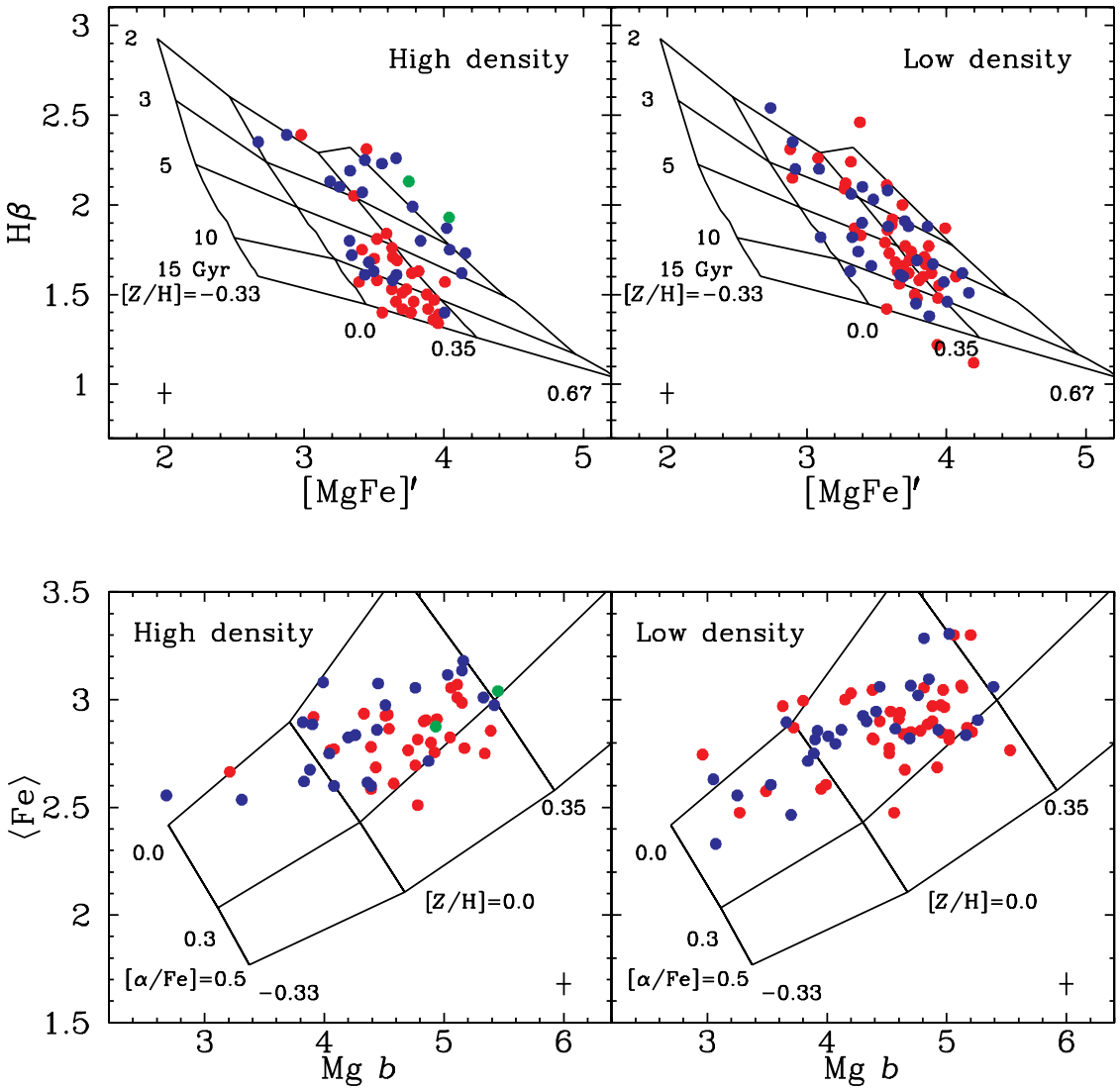

FIG. 12.—Same as Fig. 2, but the models are corrected for the decrease of O/Fe with increasing metallicity at supersolar metallicity in the solar neighborhood assuming oxygen and the other α-elements being separated.

evolution of the scaling relations of early-type galaxies (e.g., Bower et al. 1992; Aragón-Salamanca et al. 1993; Bender et al. 1993; 1996; Renzini & Ciotti 1993; Kodama et al. 1999; Ziegler et al. 1999, 2001; Saglia et al. 2000; see review by Peebles 2002). It has been known since these early (and some more recent) works that the formation ages of the stellar populations in elliptical galaxies have to be above redshifts $z \gtrsim 2$. New in this paper is the detailed disentanglement of star formation histories as a function of galaxy mass and the distinction between dense and loose environments.

We confirm such high formation redshifts for intermediate-mass and massive ($M_* \gtrsim 10^{10}\ M_\odot$ or $\sigma \gtrsim 140$ km s^{-1}) early-type galaxies in dense environments, in good agreement as well with the recently discovered relationship between globular cluster color and galaxy luminosity (Strader et al. 2004) and the *K*-*z* relation of powerful radio galaxies (Rocca-Volmerange et al. 2004). We find, however, that elliptical galaxies in looser environments form at somewhat lower redshifts between $z \sim 2$ and 1. Low-mass galaxies ($M_* \lesssim 2 \times 10^{10}\ M_\odot$ or $\sigma \lesssim 140$ km s^{-1}) in low-density regions apparently suffer from significant star formation episodes below redshift $z \sim 1$. This paper further adds the conclusion that the stellar populations of more massive early-type galaxies form earlier and faster. This result confirms early, more qualitative estimates by Bender et al. (1996) based on the redshift evolution of the Mg-σ relation, who had already noted that the formation redshifts of the most massive early-type galaxies in clusters may even be above $z \gtrsim 4$. Here we find that while the formation epoch is delayed in low-density environments by about 2 Gyr, the timescale is independent of the environmental density and depends only on the galaxy's mass concentration.

7.3. *The Stellar Mass Density at $z > 1$*

The above evidence provides consistent constraints on the epochs when the stellar populations of early-type galaxies have formed. Our results imply that at redshift around $z \sim 1$, the formation of the total stellar mass in early-type galaxies with $M_* \gtrsim 2 \times 10^{10}\ M_\odot$ or $\sigma \gtrsim 140$ km s^{-1} in both high-and low-density environments is almost completed. Stellar mass growth in early-type galaxies below redshift $z \sim 1$ is restricted to low-mass objects in low-density environments. As the latter make up only a small fraction of the total mass of a galaxy population, despite their being numerous, we can infer that stellar mass growth in early-type galaxies is largely completed around redshift $z \sim 1$.

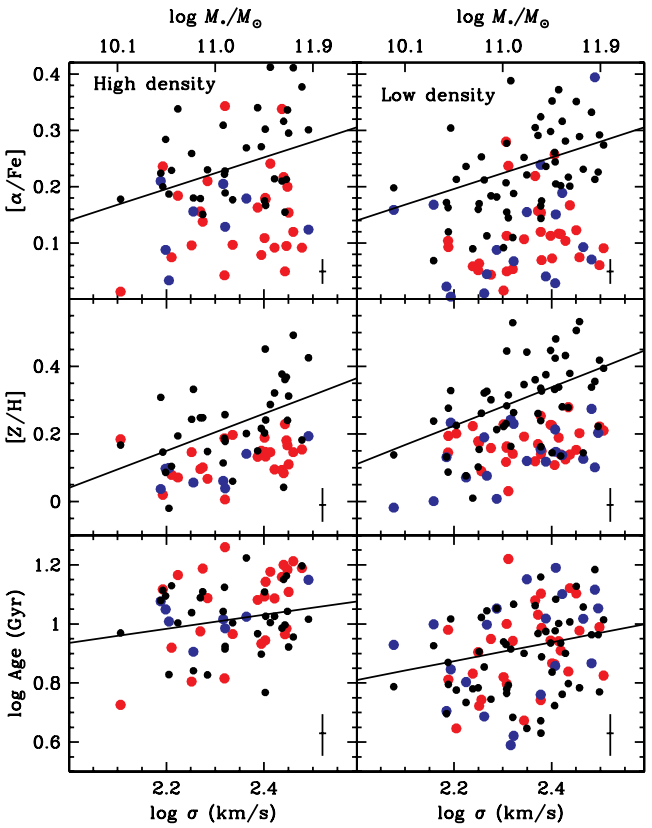

FIG. 13.—Stellar population parameters as a functions of velocity dispersion (measured within $1/10r_e$) and stellar mass (upper x-axis) for the old subpopulation (see Fig. 6). Ages and element abundances are derived with the SSP model of Fig. 11. Black points represent Monte Carlo simulations assuming eq. (1) (*solid lines*), which reproduce the data in Fig. 6.

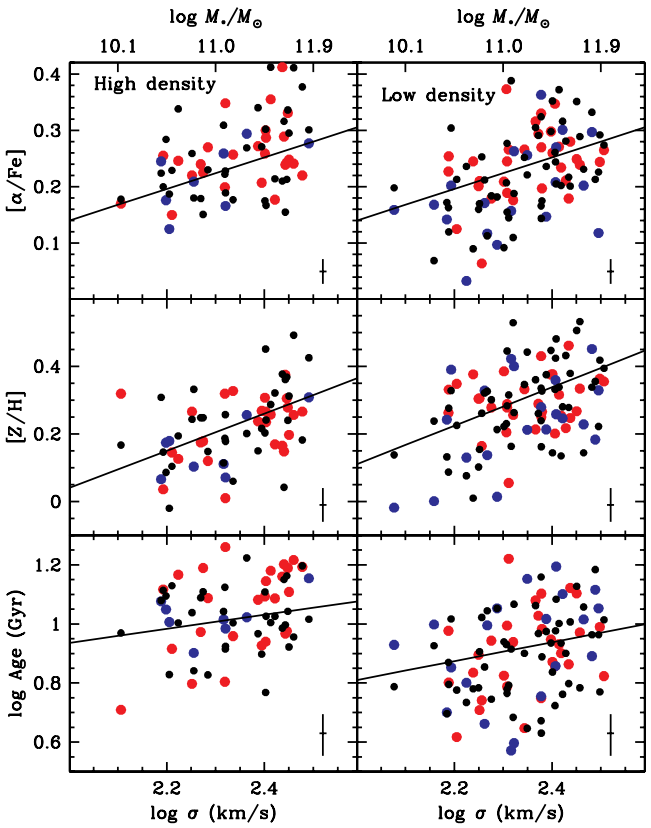

FIG. 14.—Same as Fig. 13, but ages and element abundances are derived with the SSP model of Fig. 12.

This galaxy type is expected to host between $\frac{1}{2}$ and $\frac{3}{4}$ of the total stellar mass in the universe (Renzini 1999; Bell et al. 2003). Because massive disks are also already present at redshifts between 1 and 2 (Ravindranath et al. 2004; Stockton et al. 2004), this implies that at least 50% of the total stellar mass density must have already been formed by $z \sim 1$. Our results further suggest that a significant increase of the stellar mass density between redshifts 1 and 2 should be present, caused mainly by the field galaxy population, while at redshifts around 3 the stellar mass density should be dominated by galaxies in high-density environments. Depending on the exact partition between objects in high and low environmental densities, this implies the stellar mass density around redshift 3 to be as low as 10%–30% of the local value. Observational estimates of the total stellar mass density as a function of redshift are in overall good agreement with this result. Recent studies are consistent with only mild evolution of the order of 20%–30% up to $z \sim 1$ followed by a significant drop in stellar mass density between redshifts 1 and 2 (Brinchmann & Ellis 2000; Cohen 2002; Bell et al. 2003; Dickinson et al. 2003; Fontana et al. 2003, 2004; Rudnick et al. 2003; Glazebrook et al. 2004). Our result suggests that the significant mass growth in the early-type galaxy population below $z \sim 1$ observed by Bell et al. (2004) is most likely caused by less massive objects.

7.4. *Climbing up the Redshift Ladder*

One fundamental consequence from the results of this paper is the prediction that very massive objects ($M_* \gtrsim 10^{11}\ M_\odot$) with very high star formation rates up to several 1000 $M_\odot$ yr^{-1} should be present between redshifts 2 and 5. Such objects have indeed been found recently. At least a portion of the SCUBA sources at $2 \leq z \leq 3$ turn out to be massive star-forming galaxies with extremely high star formation rates up to several thousand $M_\odot$ yr^{-1} (Smail et al. 2002; Genzel et al. 2003; Tecza et al. 2004). These objects are likely to be the precursors of the most massive elliptical galaxies ($M_* \approx 10^{12}\ M_\odot$) forming in a violent star formation episode at high redshift. Lyman break galaxies, instead, exhibit more moderate star formation rates of the order of a few times 10 $M_\odot$ yr^{-1} (Pettini et al. 2001; Baker et al. 2004) and may therefore be the precursors of less massive early-type galaxies in Figure 10 ($M_* \approx 10^{11}\ M_\odot$) and/or spiral bulges. Moreover, Pettini et al. (2002) find cB 58 (a lensed galaxy at redshift $z = 2.73$; Seitz et al. 1998) to have a significantly α-enhanced *interstellar medium*, which is in good agreement with the α/Fe enhancement derived in this paper for the *stellar population* of local elliptical galaxies.

A further direct inference from Figure 10 is that massive old, passively evolved galaxies should exist at intermediate redshifts between 1 and 2. Again, these objects have been found. Medium-deep infrared surveys detect a relatively large number of so-called extremely red objects (EROs) between $z \sim 1$ and 1.5, whose SEDs best fit evolved stellar populations (Pozzetti & Mannucci 2000; Daddi et al. 2000; Cimatti et al. 2003, 2004; Saracco et al. 2003, 2005; Väisänen & Johansson 2004; Moustakas et al. 2004; Caputi et al. 2004a). The evolved K-selected EROs mentioned above show evidence for strong clustering (Daddi et al. 2003) and hence are likely candidates for being the precursors of the cluster objects shown in Figure 10 (*top*). In a recent paper, Pierini et al. (2004) show that the colors of some "evolved" EROs are also consistent with a dusty *post*-starburst

population with ages around 0.5 Gyr, which fits the star formation histories shown in Figure 10 for the low-density environment. It would be interesting to investigate the clustering properties of this subclass of EROs to verify that they preferably are found in low-density environments. Also in agreement with our result is the recent finding in *K*-selected galaxy surveys that the most luminous objects are best fitted by older stellar populations at all redshifts up to $z \sim 1$, which implies the typical M/L ratio (in K) of more massive galaxies to be larger than that of less massive ones (Fontana et al. 2004; Glazebrook et al. 2004).

Finally, deeper redshift surveys are now finding evolved objects even at redshifts around 2 and 3 (Franx et al. 2003; Chen & Marzke 2004; McCarthy et al. 2004; Caputi et al. 2004b) and massive star-forming objects around redshifts 2 and 5 (Totani et al. 2001; Lehnert & Bremer 2003; de Mello et al. 2004) up to $z \sim 6.5$ (Kurk et al. 2004), again in good agreement with the prediction from the properties of local galaxies made in this paper. To conclude, it seems that the two approaches, archaeology of stellar populations in local galaxies and redshift surveys, are converging to a consistent picture in which massive galaxy formation occurs at fairly high redshifts accompanied by violent star formation.

7.5. *Models of Galaxy Formation*

This consistent picture of high formation redshifts of the stellar populations in massive (early-type) galaxies severely challenges the conventional semianalytic models of galaxy formation (Kauffmann et al. 1993; Somerville & Primack 1999; Cole et al. 2000; Hatton et al. 2003; Menci et al. 2004), and their modification has become unavoidable. As reviewed by Somerville (2005), recent renditions of both semianalytic models and hydrodynamical simulations of hierarchical galaxy formation (Nagamine et al. 2004) are consistent with the stellar mass function around $z = 1$ and with the cosmic star formation history (see also Fontana et al. 2004); hence, global quantities are well reproduced. However, the models have difficulty producing the high average ages of massive galaxies in the local universe and, accordingly, the number density of luminous red galaxies at intermediate redshift, as well as the high star formation rates in massive objects at high redshifts (Somerville 2005; Somerville et al. 2004).

At least part of the reason for this shortfall may be connected to the way nonbaryonic dark matter and baryonic matter are linked. In current models, star formation is tightly linked to the assembly history of dark matter halos, so that galaxies with longer assembly times also form stars on longer timescales. A possible solution to reconcile extended assembly times with fast star formation histories is a scenario in which massive objects form their stars early and assemble later (Bower et al. 1998; van Dokkum et al. 1999). This picture gets some theoretical support from the fact that the kinematics of massive early-type galaxies requires the origin of mergers between bulge-dominated rather than disk galaxies (Naab & Burkert 2003; Khochfar & Burkert 2003). However, in this case, it would be difficult for early-type galaxies to establish the correlation between metallicity and mass reported here. More fundamental modifications of the models are certainly necessary.

Granato et al. (2001) have presented a promising—even though quite heuristic—approach, in which star formation is enhanced in massive systems because of feedback between star formation and active galactic nucleus (AGN) activity (see also Cattaneo & Bernardi 2003; Kawata & Gibson 2004). This idea is now put on physical grounds in Granato et al. (2004), where the evolution of gas in a dark matter halo is described as a function of gravity, radiative cooling, heating by feedback from supernovae, and—most importantly—heating by feedback from the growing active nucleus. The assumption of a tight interplay between star formation and nuclear activity indeed gets strong observational support from the fact that besides the α/Fe ratio, black hole mass also correlates with velocity dispersion and galaxy mass (Gebhardt et al. 2000; Ferrarese & Merritt 2000). The resulting "antihierarchical baryonic collapse" in the Granato et al. (2004) model leads to higher formation redshifts and shorter formation timescales of the stellar populations in massive halos. In this way the relationship between the α/Fe ratio and galaxy mass (Romano et al. 2002), as well as the presence of old galaxies at $z \sim 1$ (EROs) and of violently star forming objects at $z \sim 3$ (SCUBA sources), is reproduced.

Granato et al. (2004) consider the evolution of massive halos in the framework of semianalytic models only above redshifts $z \gtrsim 1$. Hence, a fundamental problem that remains to be solved is the accretion of cold gas onto the central galaxy of a dark matter halo at lower redshift leading to late star formation and the galaxy's rejuvenation. An important step to a solution of this latter problem might have been recently made by Binney (2004), who suggests a scenario in which gas cooling is the key process. Unlike small systems with shallow potential wells, massive galaxies cannot eject but retain their hot gas, the cooling of which is inhibited by an episodically active galactic nucleus. This "atmosphere" of hot gas builds up a shield around the galaxy, preventing cool gas from falling in and forming stars. The inclusion of this effect in semianalytic models of hierarchical galaxy formation would certainly be the right step toward reconciling our current understanding of galaxy formation with the observational constraints set by the stellar population properties of massive galaxies.

8. CONCLUSIONS

We study the stellar population properties of 124 early-type galaxies (González 1993; Beuing et al. 2002; Mehlert et al. 2003) with velocity dispersions between 50 and 350 km s^{-1} in both high- and low-density environments. From the absorption-line indices Hβ, Mg b, and $\langle$Fe$\rangle$ we derive ages, metallicities Z/H, and α/Fe element ratios using our abundance ratio–sensitive stellar population models (TMB). The α/Fe ratio is the key to determining the formation timescales of the objects, as it quantifies the relative importance of the chemical enrichment from Type II and delayed Type Ia supernovae. Together with average ages, we use this information to set constraints on the epochs when early-type galaxies form the bulk of their stars. To get a handle on the effect of correlated errors, we compare the observed sample with mock galaxy samples with properties as close as possible to the observational data in terms of sample size, velocity dispersion distribution, and measurement errors.

For the bulk of the sample we find that all three stellar population parameters, age, total metallicity, and α/Fe ratio, correlate with velocity dispersion and hence galaxy mass. We show that these results are robust against recent revisions of the local abundance pattern at high metallicities. To recover the observed scatter, we need to assume an intrinsic scatter of about 20% in age, 0.08 dex in [Z/H], and 0.05 dex in [α/Fe]. Both zero point and slope of the α/Fe-σ relation are independent of the environmental density, while the ages of objects in low-density environments appear systematically lower accompanied by slightly higher metallicities.

We identify three classes of "outliers" from these relationships: (1) The low-mass objects with $M_* \lesssim 10^{10}\ M_\odot$ ($\sigma < 130$ km s^{-1})

in our sample show clear evidence for the presence of intermediate-age populations. Their line indices are best reproduced by a two-component model in which a 1.5–2 Gyr population with low α/Fe ratios is added to a base population defined by the above relationships. (2) About 20% of the intermediate-mass objects with $10^{10} \lesssim M_*/M_\odot \lesssim 10^{11}$ [$110 \lesssim \sigma/(\mathrm{km\ s^{-1}}) \lesssim 230$] must have either a young subpopulation or a blue horizontal branch. Compared to the low-mass objects, the case for the intermediate-age population is less convincing because of relatively high α/Fe ratios. (3) Most intriguing is a population of massive ($M_* \gtrsim 10^{11}\ M_\odot$ or $\sigma \gtrsim 200$ km s^{-1}) S0 galaxies, only present in the high-density sample, that require a major fraction of their stars ($\sim$70%) to have formed relatively recently at look-back times of about 2–3 Gyr, corresponding to $z \sim 0.2$. Note that these objects, although interesting in themselves, represent only a minor fraction of the total stellar mass budget in early-type galaxies.

The increase of total metallicity, indicating the completeness of chemical processing, mainly reflects the inability of massive galaxies with deeper potential wells to develop galactic winds. The increase of age and α/Fe ratio with σ shows that more massive galaxies form their stellar populations both earlier and faster. Our results suggest that the well-known Mg-σ relation is mainly driven by metallicity ($\sim$60% contribution) with an almost equal share from α/Fe ratio ($\sim$23%) and age ($\sim$17%). The increase of α/Fe with velocity dispersion is responsible for the much weaker correlation of $\langle$Fe$\rangle$ with galaxy mass.

With a simple chemical evolution model that takes the delayed enrichment from Type Ia supernovae into account, we translate the ages and α/Fe ratios of the above relationships into star formation histories as a function of a galaxy's velocity dispersions and environmental densities. We show that the higher ages and α/Fe ratios of more massive early-type galaxies imply faster formation timescales at earlier epochs. The lower the mass of a galaxy is, the more it suffers from episodes of late star formation extending to redshifts below $z \sim 1$ for galaxies with $M_* \lesssim 10^{10}\ M_\odot$. Massive early-type galaxies ($M_* \gtrsim 10^{11}\ M_\odot$) in high-density environments form their stellar populations between redshifts 2 and 5. Galaxies in low-density environments appear on average 1–2 Gyr younger than their counterparts in high environmental densities but obey the same relationship between α/Fe ratio and velocity dispersion. This implies that they form on the same timescales, but the epochs of their formation are delayed to lower redshifts between $z \sim 1$ and 2.

The "archaeology approach" pursued in this paper and observations of the high-redshift universe are now converging to a consistent picture. The results of this work imply that at least 50% of the total stellar mass density must have already been formed by $z \sim 1$, which is in good agreement with observational estimates of the total stellar mass density as a function of redshift. We conclude that significant mass growth in the early-type galaxy population below $z \sim 1$ must be restricted to less massive objects, and a significant increase of the stellar mass density between redshifts 1 and 2 should be present, caused mainly by the field galaxy population. As shown here, the properties of local galaxies predict the presence of massive objects with very high star formation rates of the order of 1000 $M_\odot$ yr^{-1} around redshifts 2–5, as well as the existence of old evolved galaxies at redshifts between 1 and 2, both now confirmed observationally.

Current models of hierarchical galaxy formation are consistent with global properties such as the stellar mass function but remain challenged by the ages of local massive galaxies, the number densities of luminous red objects at intermediate redshift, and the high star formation rates in massive objects at high redshifts. The problem seems tightly linked to the (uncertain) treatment of baryonic matter in dark halos, and likely solutions lie in the inclusion of AGN feedback and refinement of gas heating/cooling processes.

We thank the referee, Robert Proctor, for his careful reading of the manuscript and for his very constructive report.

APPENDIX A

DATA SAMPLE

In Table 2 we list velocity dispersions, line indices Hβ, Mg b, and $\langle$Fe$\rangle$, galaxy types, environmental densities, literature sources, and classifications of Figure 4 for the sample investigated. Table 3 gives the stellar population parameters age, metallicity, and α/Fe ratio derived with the TMB models. The 1 σ errors are estimated through Monte Carlo simulations. We perturb the line indices assuming a Gaussian probability distribution defined by the 1 σ measurement errors quoted above. The resulting 1 σ errors correspond to the widths of the distributions in the stellar population parameters from 100 Monte Carlo realizations per object.

APPENDIX B

THE LOCAL ABUNDANCE PATTERN AT HIGH METALLICITIES

As mentioned in § 7.1, Proctor et al. (2004b) argue that the correlation of α/Fe with velocity dispersion is an "artefact of incomplete calibration (of the models) to the Lick system." This argument is based on the recent finding of Bensby et al. (2004) that the Milky Way disk stars with supersolar metallicities do not have solar but subsolar O/Fe ratios, with O/Fe decreasing with increasing Fe/H (see also Pompéia et al. 2003; Allende Prieto et al. 2004).

We investigated this issue constructing two additional flavors of stellar population models that account for the local abundance pattern at high metallicity: one in which oxygen is taken as representative of all α-elements assuming these elements to be enriched in lockstep (as in Proctor et al. 2004b) and one in which oxygen is detached from the rest of the α-elements as discussed above. The decrease of O/Fe with metallicity is adopted directly from Bensby et al. (2004) and can be parameterized as (Proctor et al. 2004b)

$$[\mathrm{O/Fe}] = -0.5[\mathrm{Fe/H}] \qquad \text{for} \qquad [\mathrm{Fe/H}] > 0. \tag{B1}$$

B1. OXYGEN AND α-ELEMENTS IN LOCKSTEP

The resulting model in the index-index planes, assuming oxygen as a representative for all α-elements, is shown in Figure 11 (equivalent to Fig. 2). The effect is striking. Since oxygen dominates metallicity, the correction for the subsolar O/Fe of the calibrating stars at high metallicities has the effect that the models are practically "labeled" with lower metallicities. As a consequence, stronger metal indices at a given metallicity are predicted, which leads to the derivation of somewhat lower (but still supersolar) metallicities (Fig. 11, *top*). The derived ages, instead, remain unchanged. Even more dramatic is the modification of the model in the Mg b–$\langle$Fe$\rangle$ plane (Fig. 11, *bottom*). At supersolar metallicity, the O/Fe (hence α/Fe in this case) of the original model based on the local abundance pattern has to be increased in order to obtain solar-scaled abundance ratios. This is achieved mainly by decreasing the abundance of iron, so that the iron indices get weaker and the Mg b index get stronger (because of the inverse response to Fe abundance; see TMB for details). The model slope in this diagram is now close to the slope of the data, which clearly affects the derived α/Fe–σ relation.

For a better illustration, the stellar population parameters of the galaxy sample investigated here obtained with this model are plotted in Figure 13 (the equivalent to Fig. 6). The relationships of equation (1) plus the Monte Carlo realizations of Figure 6 are also shown for comparison. The α/Fe ratios are lower by about 0.1 dex, and in particular the α/Fe–σ relation disappears. Metallicities are also lower by about 0.1 dex, and the Z/H–σ relationship gets significantly tighter. These findings are in agreement with the conclusions of Proctor et al. (2004b). Note that the ages do not change.

B2. OXYGEN AND α-ELEMENTS SEPARATED

In this second flavor of the model we account for the fact that the other α-elements (in particular magnesium) actually do not follow the decrease of the local O/Fe ratio with increasing metallicity at supersolar metallicities (Bensby et al. 2004); hence, $[\mathrm{Ne, Mg, Si, S, Ar, Ca, Ti/Fe}] = 0$ for $[\mathrm{Fe/H}] \geq 0$. The impact on the index-index diagrams is shown in Figure 12. The model is almost indistinguishable from the original model used for the analysis of this paper (Fig. 2) and very different from the model in which oxygen and the other α-elements are lumped together (Fig. 11). The reason is the following. Oxygen contributes almost one-half and the rest of the α-elements about one-quarter to total metallicity. A variation of the α/Fe ratio *including oxygen* is therefore obtained mainly by a modification of Fe abundance (Trager et al. 2000a; TMB).

The correction from the local subsolar O/Fe to solar element ratios is therefore achieved by a decrease of Fe abundance by 40%. When oxygen is detached from the other α-elements, instead, the picture is very different. The required decrease of Fe abundance is only 20%, which reduces both the decrease of the Fe indices and the increase of Mg b (note that Mg b responds inversely to Fe abundance). On top of this, the abundances of the other α-elements (including magnesium) need to be reduced by the same amount to maintain the solar α/Fe ratio. This leads to a further decrease of Mg b and an increase of the Fe indices, the latter being inversely coupled with Mg abundance (Tripicco & Bell 1995; Korn et al. 2004). The effect is sufficient to bring the model back to its original position. As a consequence, the stellar population parameters derived with this model are in excellent agreement with the ones presented in this work, as shown in Figure 14.

To conclude, when the nonsolar O/Mg ratios of metal-rich stars in the solar neighborhood are taken into account, the correction for the local abundance pattern has no significant impact on the model. This implies that the results of this paper are robust against this problem. In particular, the α/Fe–σ relation found here is real and not caused by calibration artifacts.

REFERENCES

Allende Prieto, C., Barklem, P. S., Lambert, D. L., & Cunha, K. 2004, A&A, 420, 183
Aragón-Salamanca, A., Ellis, R. S., Couch, W. J., & Carter, D. 1993, MNRAS, 262, 764
Arimoto, N., & Yoshii, Y. 1987, A&A, 173, 23
Baker, A. J., Tacconi, L. J., Genzel, R., Lehnert, M. D., & Lutz, D. 2004, ApJ, 604, 125
Baldry, I. K., Glazebrook, K., Brinkmann, J., Ivezić, Ž., Lupton, R. H., Nichol, R. C., & Szalay, A. S. 2004, ApJ, 600, 681
Bell, E., McIntosh, D. H., Katz, N., & Weinberg, M. D. 2003, ApJS, 149, 289
Bell, E. F., et al. 2004, ApJ, 608, 752
Bender, R. 1988, A&A, 202, L5
Bender, R., Burstein, D., & Faber, S. M. 1992, ApJ, 399, 462
———. 1993, ApJ, 411, 153
Bender, R., & Paquet, A. 1995, in IAU Symp. 164, Stellar Populations, ed. P. C. van der Kruit & G. Gillmore (Dordrecht: Kluwer), 259
Bender, R., Ziegler, B. L., & Bruzual, G. 1996, ApJ, 463, L51
Bensby, T., Feltzing, S., & Lundström, I. 2003, A&A, 410, 527
———. 2004, A&A, 415, 155
Bernardi, M., Renzini, A., da Costa, L. N., Wegner, G., Alonso, M. V., Pellegrini, P. S., Rité, C., & Willmer, C. N. A. 1998, ApJ, 508, L143
Bernardi, M., et al. 2003, AJ, 125, 1882
Beuing, J., Bender, R., Mendes de Oliveira, C., Thomas, D., & Maraston, C. 2002, A&A, 395, 431
Binney, J. 2004, MNRAS, 347, 1093
Bower, R., Kodama, T., & Terlevich, A. 1998, MNRAS, 299, 1193
Bower, R. G., Lucey, J. R., & Ellis, R. S. 1992, MNRAS, 254, 589
Brinchmann, J., & Ellis, R. S. 2000, ApJ, 536, L77
Caldwell, N., Rose, J. A., & Concannon, K. D. 2003, AJ, 125, 2891
Caputi, K. I., Dunlop, J. S., McLure, R. J., & Roche, N. D. 2004a, MNRAS, 353, 30
———. 2004b, MNRAS, submitted (astro-ph/0408373)
Carollo, C. M., & Danziger, I. J. 1994, MNRAS, 270, 523
Carter, D., et al. 2002, ApJ, 567, 772
Cattaneo, A., & Bernardi, M. 2003, MNRAS, 344, 45
Cenarro, A. J., Gorgas, J., Vazdekis, A., Cardiel, N., & Peletier, R. F. 2003, MNRAS, 339, L12
Chen, H., & Marzke, R. 2004, ApJ, 615, 603
Chiosi, C., & Carraro, G. 2002, MNRAS, 335, 335
Cimatti, A., et al. 2003, A&A, 412, L1
———. 2004, Nature, 430, 184
Cohen, J. G. 2002, ApJ, 567, 672
Cole, S., Lacey, C. G., Baugh, C. M., & Frenk, C. S. 2000, MNRAS, 319, 168
Colless, M., Burstein, D., Davies, R. L., McMahan, R. K., Saglia, R. P., & Wegner, G. 1999, MNRAS, 303, 813
Daddi, E., et al. 2000, A&A, 361, 535
———. 2003, ApJ, 588, 50
Davies, R. L., Sadler, E. M., & Peletier, R. F. 1993, MNRAS, 262, 650
Davies, R. L., et al. 2001, ApJ, 548, L33
de Freitas Pacheco, J. A., & Barbuy, B. 1995, A&A, 302, 718
De Lucia, G., et al. 2004, ApJ, 610, L77
de Mello, D. F., Daddi, E., Renzini, A., Cimatti, A., di Serego Alighieri, S., Pozzetti, L., & Zamorani, G. 2004, ApJ, 608, L29
Dickinson, M., Papovich, C., Ferguson, H. C., & Budavári, T. 2003, ApJ, 587, 25
Djorgovski, S., & Davis, M. 1987, ApJ, 313, 59
Dressler, A., Lynden-Bell, D., Burstein, D., Davies, R. L., Faber, S. M., Terlevich, R. J., & Wegner, G. 1987, ApJ, 313, 42
Edmunds, M. G. 1990, MNRAS, 246, 678

Faber, S. M., Friel, E. D., Burstein, D., & Gaskell, D. M. 1985, ApJS, 57, 711
Faber, S. M., & Jackson, R. E. 1976, ApJ, 204, 668
Ferrarese, L., & Merritt, D. 2000, ApJ, 539, L9
Fisher, D., Franx, M., & Illingworth, G. 1995, ApJ, 448, 119
Fontana, A., et al. 2003, ApJ, 594, L9
———. 2004, A&A, 424, 23
Franx, M., & Illingworth, G. D. 1988, ApJ, 327, L55
Franx, M., et al. 2003, ApJ, 587, L79
Fuhrmann, K. 1998, A&A, 338, 161
Fusi-Pecci, F., & Renzini, A. 1975, A&A, 39, 413
———. 1976, A&A, 46, 447
Gavazzi, G., Bonfanti, C., Sanvito, G., Boselli, A., & Scodeggio, M. 2002, ApJ, 576, 135
Gebhardt, K., et al. 2000, ApJ, 539, L13
———. 2003, ApJ, 597, 239
Genzel, R., Baker, A. J., Tacconi, L. J., Lutz, D., Cox, P., Guilloteau, S., & Omont, A. 2003, ApJ, 584, 633
Glazebrook, K., et al. 2004, Nature, 430, 181
González, J. 1993, Ph.D. thesis, Univ. California, Santa Cruz
Gorgas, J., Efstathiou, G., & Aragón Salamaca, A. 1990, MNRAS, 245, 217
Granato, G. L., De Zotti, G., Silva, L., Bressan, A., & Danese, L. 2004, ApJ, 600, 580
Granato, G. L., Silva, L., Monaco, P., Panuzzo, P., Salucci, P., De Zotti, G., & Danese, L. 2001, MNRAS, 324, 757
Greggio, L. 1997, MNRAS, 285, 151
Greggio, L., & Renzini, A. 1983, A&A, 118, 217
———. 1990, ApJ, 364, 35
Hatton, S., Devriendt, J. E. G., Ninin, S., Bouchet, F. R., Guiderdoni, B., & Vibert, D. 2003, MNRAS, 343, 75
Hau, G. K. T., Carter, D., & Balcells, M. 1999, MNRAS, 306, 437
Jimenez, R., Panter, B., Heavens, A. F., & Verde, L. 2005, MNRAS, 356, 495
Jørgensen, I. 1999, MNRAS, 306, 607
Jørgensen, I., Franx, M., & Kjærgaard, P. 1995, MNRAS, 276, 1341
Kauffmann, G., & Charlot, S. 1998, MNRAS, 294, 705
Kauffmann, G., White, S. D. M., & Guiderdoni, B. 1993, MNRAS, 264, 201
Kawata, D., & Gibson, B. K. 2004, MNRAS, submitted (astro-ph/0409068)
Kelson, D. D., Illingworth, G. D., van Dokkum, P. G., & Franx, M. 2000, ApJ, 531, 137
Khochfar, S., & Burkert, A. 2003, ApJ, 597, L117
Kobayashi, C., & Arimoto, N. 1999, ApJ, 527, 573
Kodama, T., & Arimoto, N. 1997, A&A, 320, 41
Kodama, T., Bower, R. G., & Bell, E. F. 1999, MNRAS, 306, 561
Korn, A., Maraston, C., & Thomas, D. 2004, A&A, submitted
Kuntschner, H. 2000, MNRAS, 315, 184
Kuntschner, H., & Davies, R. L. 1998, MNRAS, 295, L29
Kuntschner, H., Lucey, J. R., Smith, R. J., Hudson, M. J., & Davies, R. L. 2001, MNRAS, 323, 615
Kuntschner, H., Smith, R. J., Colless, M., Davies, R. L., Kaldare, R., & Vazdekis, A. 2002, MNRAS, 337, 172
Kurk, J. D., Cimatti, A., di Serego Alighieri, S., Vernet, J., Daddi, E., Ferrara, A., & Ciardi, B. 2004, A&A, 422, L13
Lauberts, A., & Valentijn, E. A. 1989, The Surface Photometry Catalogue of the ESO-Upsalla Galaxies (Garching: ESO)
Lee, H., Yoon, S., & Lee, Y. 2000, AJ, 120, 998
Lehnert, M. D., & Bremer, M. 2003, ApJ, 593, 630
Leitherer, C. 1998, in ASP Conf. Ser. 142, The Stellar Initial Mass Function, ed. G. Gilmore & D. Howell (San Francisco: ASP), 61
Longhetti, M., Bressan, A., Chiosi, C., & Rampazzo, R. 2000, A&A, 353, 917
Maraston, C. 1998, MNRAS, 300, 872
———. 2004, MNRAS, submitted
———. 2005, in Multiwavelength Mapping of Galaxy Formation and Evolution, ed. R. Bender & A. Renzini (Berlin: Springer), in press (astro-ph/0402269)
Maraston, C., Greggio, L., Renzini, A., Ortolani, S., Saglia, R. P., Puzia, T., & Kissler-Patig, M. 2003, A&A, 400, 823
Maraston, C., Kissler-Patig, M., Brodie, J. P., Barmby, P., & Huchra, J. 2001, A&A, 370, 176
Maraston, C., & Thomas, D. 2000, ApJ, 541, 126
Mateo, M. L. 1998, ARA&A, 36, 435
Matteucci, F. 1994, A&A, 288, 57
Matteucci, F., & Greggio, L. 1986, A&A, 154, 279
McCarthy, P. J., et al. 2004, ApJ, 614, L9
McWilliam, A. 1997, ARA&A, 35, 503
Mehlert, D., Saglia, R. P., Bender, R., & Wegner, G. 1998, A&A, 332, 33
———. 2000, A&AS, 141, 449
Mehlert, D., Thomas, D., Saglia, R. P., Bender, R., & Wegner, G. 2003, A&A, 407, 423
Menci, N., Cavaliere, A., Fontana, A., Giallongo, E., Poli, F., & Vittorini, V. 2004, ApJ, 604, 12
Merluzzi, P., La Barbera, F., Massarotti, M., Busarello, G., & Capaccioli, M. 2003, ApJ, 589, 147
Moustakas, L. A., et al. 2004, ApJ, 600, L131
Naab, T., & Burkert, A. 2003, ApJ, 597, 893
Nagamine, K., Cen, R., Hernquist, L., Ostriker, J. P., & Springel, V. 2004, ApJ, 610, 45
Nomoto, K., Thielemann, F.-K., & Yokoi, K. 1984, ApJ, 286, 644
Pagel, B. E. J., & Tautvaisiene, G. 1995, MNRAS, 276, 505
Peebles, P. J. E. 2002, in ASP Conf. Ser. 283, A New Era in Cosmology, ed. N. Metcalfe & T. Shanks (San Francisco: ASP), 351
Peletier, R. 1989, Ph.D. thesis, Rijksuniv. Groningen
Pettini, M., Rix, S. A., Steidel, C. C., Adelberger, K. L., Hunt, M. P., & Shapley, A. E. 2002, ApJ, 569, 742
Pettini, M., Shapley, A. E., Steidel, C. C., Cuby, J., Dickinson, M., Moorwood, A. F. M., Adelberger, K. L., & Giavalisco, M. 2001, ApJ, 554, 981
Pierini, D., Maraston, C., Bender, R., & Witt, A. N. 2004, MNRAS, 347, 1
Pipino, A., & Matteucci, F. 2004, MNRAS, 347, 968
Poggianti, B. M., Smail, I., Dressler, A., Couch, W. J., Barger, A. J., Butcher, H., Ellis, R. S., & Oemler, A. J. 1999, ApJ, 518, 576
Poggianti, B., et al. 2001a, ApJ, 562, 689
———. 2001b, ApJ, 563, 118
Pompéia, L., Barbuy, B., & Grenon, M. 2003, ApJ, 592, 1173
Pozzetti, L., & Mannucci, F. 2000, MNRAS, 317, L17
Proctor, R. N., Forbes, D. A., & Beasley, M. A. 2004a, MNRAS, 355, 1327
Proctor, R. N., Forbes, D. A., Hau, G. K. T., Beasley, M. A., De Silva, G. M., Contreras, R., & Terlevich, A. I. 2004b, MNRAS, 349, 1381
Proctor, R. N., & Sansom, A. E. 2002, MNRAS, 333, 517
Puzia, T., Saglia, R. P., Kissler-Patig, M., Maraston, C., Greggio, L., Renzini, A., & Ortolani, S. 2002, A&A, 395, 45
Ravindranath, S., et al. 2004, ApJ, 604, L9
Reimers, D. 1975, Mem. Soc. R. Sci. Liège, 8, 369
Renzini, A. 1999, Ap&SS, 267, 357
Renzini, A., & Ciotti, L. 1993, ApJ, 416, L49
Renzini, A., & Voli, M. 1981, A&A, 94, 175
Rocca-Volmerange, B., Le Borgne, D., De Breuck, C., Fioc, M., & Moy, E. 2004, A&A, 415, 931
Romano, D., Silva, L., Matteucci, F., & Danese, L. 2002, MNRAS, 334, 444
Rood, R. T. 1973, ApJ, 184, 815
Rose, J. A. 1984, AJ, 89, 1238
Rose, J. A., Bower, R. G., Caldwell, N., Ellis, R. S., Sharples, R. M., & Teague, P. 1994, AJ, 108, 2054
Rudnick, G., et al. 2003, ApJ, 599, 847
Saglia, R. P., Maraston, C., Greggio, L., Bender, R., & Ziegler, B. 2000, A&A, 360, 911
Saglia, R. P., Maraston, C., Thomas, D., Bender, R., & Colless, M. 2002, ApJ, 579, L13
Sanchez-Blazquez, P., Gorgas, J., Cardiel, N., Cenarro, A. J., & González, J. J. 2003, ApJ, 590, L91
Saracco, P., et al. 2003, A&A, 398, 127
———. 2005, MNRAS, in press (astro-ph/0412020)
Schiavon, R. P., Rose, J. A., Courteau, S., & MacArthur, L. A. 2004, ApJ, 608, L33
Seitz, S., Saglia, R. P., Bender, R., Hopp, U., Belloni, P., & Ziegler, B. 1998, MNRAS, 298, 945
Silva, D. R., & Bothun, G. D. 1998, AJ, 116, 85
Smail, I., Ivison, R. J., Blain, A. W., & Kneib, J.-P. 2002, MNRAS, 331, 495
Somerville, R. 2005, in Multiwavelength Mapping of Galaxy Formation and Evolution, ed. R. Bender & A. Renzini (Berlin: Springer), in press (astro-ph/0401570)
Somerville, R. S., & Primack, J. R. 1999, MNRAS, 310, 1087
Somerville, R. S., et al. 2004, ApJ, 600, L135
Spergel, D. N., et al. 2003, ApJS, 148, 175
Stanford, S. A., Eisenhardt, P. R., & Dickinson, M. 1998, ApJ, 492, 461
Stockton, A., Canalizo, G., & Maihara, T. 2004, ApJ, 605, 37
Strader, J., Brodie, J. P., & Forbes, D. A. 2004, AJ, 127, 3431
Surma, P., & Bender, R. 1995, A&A, 298, 405
Tantalo, R., Chiosi, C., & Bressan, A. 1998, A&A, 333, 419
Tecza, M., et al. 2004, ApJ, 605, L109
Terlevich, A., & Forbes, D. 2002, MNRAS, 330, 547
Terlevich, A. I., Kuntschner, H., Bower, R. G., Caldwell, N., & Sharples, R. M. 1999, MNRAS, 310, 445
Thielemann, F.-K., Nomoto, K., & Hashimoto, M. 1996, ApJ, 460, 408
Thomas, D., Greggio, L., & Bender, R. 1998, MNRAS, 296, 119
———. 1999, MNRAS, 302, 537
Thomas, D., & Maraston, C. 2003, A&A, 401, 429
Thomas, D., Maraston, C., & Bender, R. 2002, Ap&SS, 281, 371
———. 2003a, MNRAS, 339, 897 (TMB)
———. 2003b, MNRAS, 343, 279

Thomas, D., Maraston, C., & Korn, A. 2004, MNRAS, 351, L19
Thorén, P., Edvardsson, B., & Gustafsson, B. 2004, A&A, 425, 187
Totani, T., Yoshii, Y., Iwamuro, F., Maihara, T., & Motohara, K. 2001, ApJ, 558, L87
Trager, S. C., Faber, S. M., Worthey, G., & González, J. J. 2000a, AJ, 119, 1645
———. 2000b, AJ, 120, 165
Treu, T., Stiavelli, M., Casertano, S., Møller, P., & Bertin, G. 2002, ApJ, 564, L13
Tripicco, M. J., & Bell, R. A. 1995, AJ, 110, 3035
Väisänen, P., & Johansson, P. H. 2004, A&A, 422, 453
van den Heuvel, E. P. J. 1975, ApJ, 196, L121
van Dokkum, P. G., Franx, M., Fabricant, D., Illingworth, G. D., & Kelson, D. 2000, ApJ, 541, 95
van Dokkum, P. G., Franx, M., Fabricant, D., Kelson, D. D., & Illingworth, G. D. 1999, ApJ, 520, L95
van Dokkum, P. G., Franx, M., Kelson, D. D., & Illingworth, G. D. 2001, ApJ, 553, L39
Vazdekis, A., & Arimoto, N. 1999, ApJ, 525, 144
Vazdekis, A., Kuntschner, H., Davies, R. L., Arimoto, N., Nakamura, O., & Peletier, R. F. 2001, ApJ, 551, L127
Vazdekis, A., Peletier, R. F., Beckmann, J. E., & Casuso, E. 1997, ApJS, 111, 203
Woosley, S. E., & Weaver, T. A. 1995, ApJS, 101, 181
Worthey, G. 1994, ApJS, 95, 107
———. 1998, PASP, 110, 888
Worthey, G., & Collobert, M. 2003, ApJ, 586, 17
Worthey, G., Faber, S. M., & González, J. J. 1992, ApJ, 398, 69
Ziegler, B. L., & Bender, R. 1997, MNRAS, 291, 527
Ziegler, B. L., Bower, R. G., Smail, I., Davies, R. L., & Lee, D. 2001, MNRAS, 325, 1571
Ziegler, B. L., Saglia, R. P., Bender, R., Belloni, P., Greggio, L., & Seitz, S. 1999, A&A, 346, 13